

Electronic Supplementary Information (ESI)

Utilizing ferrocene for doping Iron to graphitic carbon nitride ($\text{Fe}^{\text{II}}/\text{g-C}_3\text{N}_4$): An internal dual photocatalyst for tandem oxidation/cyclization of toluene to benzimidazoles under visible light condition

Mohammad Bashiri,¹ Yanlong Gu,² Dengyue Zheng,² Mona Hosseini-Sarvari^{1*}

¹Nanophotocatalysis Lab., Department of Chemistry, Shiraz University, Shiraz 7194684795, I.R. Iran.

² Institute of Physical Chemistry and Industrial Catalysis, School of Chemistry and Chemical Engineering, Huazhong University of Science and Technology, Luoyu Road 1037#, Hongshan District, Wuhan, 430074, P.R. China

Email:  hossaini@shirazu.ac.ir

List of Contents

Home-made photoreactor system.....	S3
Experimental section.....	S4
General Information.....	S4
Preparation of starting materials used in the synthesis of benzimidazole derivatives.....	S4
General procedure for synthesis of 1,4-bis(<i>p</i> -tolyloxy) butane.....	S4
General procedure for synthesis of 2,4,6-tris(<i>p</i> -tolyloxy)-1,3,5-triazine.....	S5
NMR (¹ H and ¹³ C) and FT-IR data of synthesized benzimidazole.....	S5
General procedure for preparation modified with g-C ₃ N ₄ and Fe ^{III} /g-C ₃ N ₄ and unmodified CPEs.	S7
Photoelectrochemical measurements.....	S7
EDX and elemental analysis investigation nanocomposite Fe ^{III} /g-C ₃ N ₄ (0.02 wt%):.....	S8
NMR (¹ H and ¹³ C) and FT-IR Spectra of compounds	S9
References	S33

Home-made photoreactor system

To the employment of visible light irradiation, low-price as well as high-energy LEDs, we resolved to illustrate an acceptable batch optical system to explore the photocatalytic properties of our synthesized nanocomposite $\text{Fe}^{\text{III}}\text{-C}_3\text{N}_4$. The Beer–Lambert rule demonstrates that the photon flux is straight corresponding to the distance, and the photon flux decreases with enhancing depth in the reaction medium¹. According to the stated facts, for photocatalytic reactions, it is very sensible that the reaction medium is near the irradiation source. We were assayed to design a united photoreactor that would introduce cooling, shaking, operational simplicity, and most importantly, highly matchable results. In this photo reactor system, several sites were fixed for the reaction medium, which was closest to the irradiation source. An interesting issue in the mentioned photo reactor system was the radiation of light from below the reaction medium. A distance of 1cm was improvised between the test tube and the LED array to absorb photons. In order to integrate mixing, a commercial-available stirrer with 2300 rpm (IKA and Heidolph) with a magnet was applied. Four LED powers (3W) were conducted in series and a total of 12W radiates to the medium reaction. LED powers (12W) with various wavelengths in the visible region were provided and put on the aluminum heatsink. Thus, the reaction medium was then irradiated with light from below. One characteristic added to the design was the facility to control the intensity of radiant light. A test tube holder set was illustrated to combine various test tube sizes such as 12-, 16-, and 20-mm tubes letting pattern reaction scales from millimolar to gram scale. These tube places verify fixed and stable placement while keeping the optimized test tube-to-LED distance. In order to chill the reaction medium and LEDs, a thermobox was utilized where water flow was feasible with a pump. Some pictures of the home-made photoreactor are displayed in Figure S1.

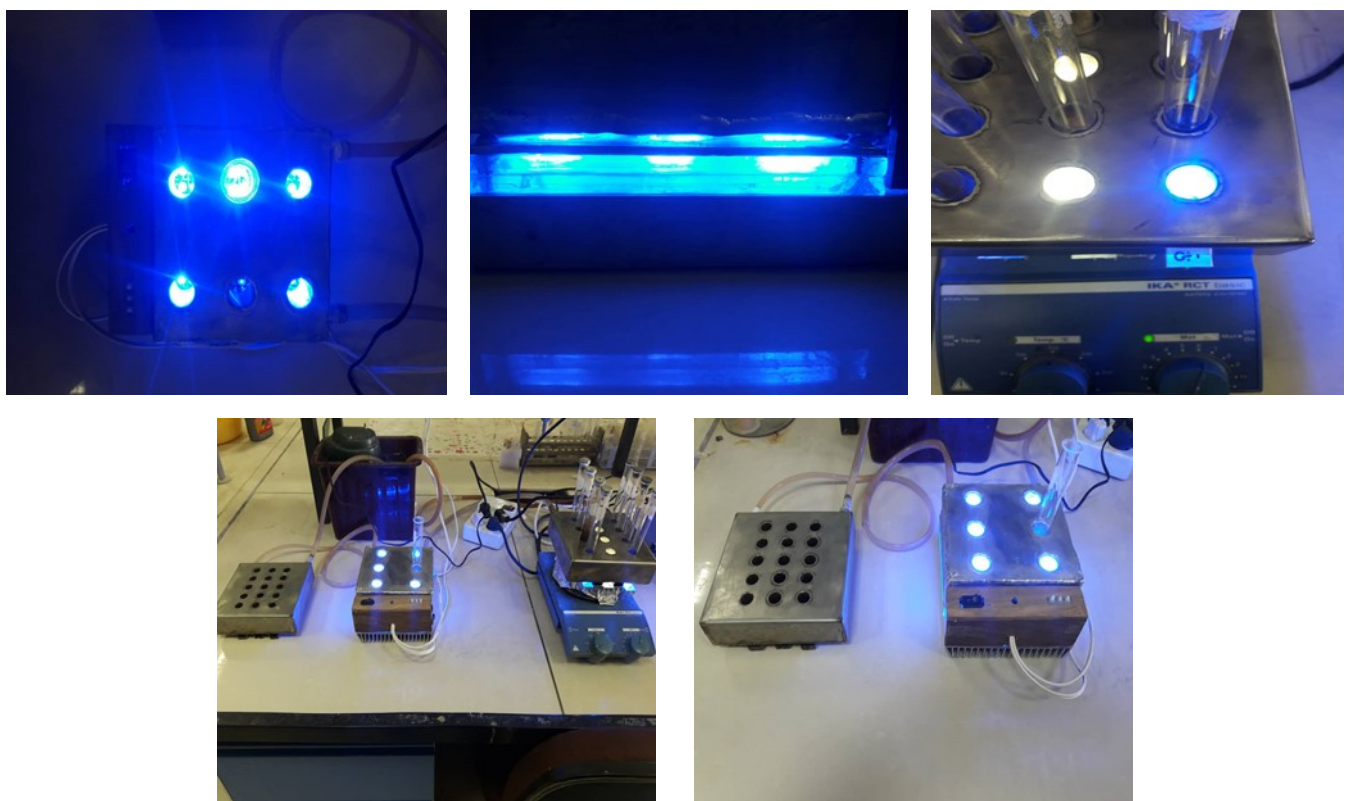


Figure S1. Newly LEDs photo reactor system to show high photon offer to the reaction medium

Experimental section:

1. General Information

All primary materials used in this article were bought from famous and basic chemical companies such as Fluka, Acros Organic, Sigma-Aldrich, Merck and which were used with no more purification. Due to the sensitivity of the reactions, all solvents were dried by appropriate methods before use. Various methods and analyses have been studied to identify the structure of prepared nanocomposites and synthesized compounds such as FT-IR test, ¹H and ¹³C nuclear magnetic resonance spectral information, X-ray diffraction analysis (XRD), X-ray fluorescence (XRF), scanning electron microscope (SEM), high-resolution transmission electron microscopy (HR-TEM), energy dispersive X-ray analysis (EDX), UV-visible DRS and photoluminescence analysis, X-ray photoelectron spectroscopy (XPS), cyclic voltammetry, Mott-Schottky, photocurrent, and electrochemical impedance spectroscopy analyses and Brunauer-Emmett-Teller surface area analysis (BET). Fourier-transform infrared spectroscopies were provided on a Tensor II Bruker spectrometer utilizing in the frequency range between 400 to 4000 (ν in cm^{-1}). The confocal Raman spectroscopy was recorded by Lab Ram HR (Horiba company, Japan). Fluorescence spectroscopy was run by Varian Cary Eclipse Fluorimeter. UV-visible DRS spectroscopy was run by Jasco V-670 absorption spectrometer. The XRF was recorded on Unisantis XMF 104. Cyclic voltammetry, Mott-Schottky, electrochemical impedance spectroscopy and photocurrent were investigated with auto lab 84490. EDX analyses were obtained by TESCAN-Vega 3. To determine the X-ray diffraction pattern of the g-C₃N₄ and nanocomposite Fe^{III}/g-C₃N₄, XRD technique was followed by applying for Bruker D-8 ADVANCE with a CuKa irradiation source (1.5406 Å). The 2θ angle was scanned at a rate of 1.5 °/min within the 2θ = 5-90°. The synthesized g-C₃N₄ and nanocomposite Fe^{III}/g-C₃N₄ were characterized by transmission electron microscopy (TEM) with Tecnai G2 F30 Manufacturer: Dutch FEI Company and scanning electron microscopy (SEM) with Sirion 200 Manufacturer: Dutch FEI Company. The XPSs of the g-C₃N₄ and nanocomposite Fe^{III}/g-C₃N₄ were characterized on a AXIS SUPRA+ Manufacturer: Shimadzu-Kratos, Japan. BET analysis was studied by Belsorp mini II from Microtrac Bel Corp company. ¹H nuclear magnetic resonance spectroscopies were run on a Bruker Avance III 400 MHz and using deuterated DMSO with tetramethylsilane as an internal standard, ¹³C nuclear magnetic resonance spectroscopies were run on a Bruker Avance III 100 MHz and using deuterated DMSO with tetramethylsilane as an internal standard. Chemical shifts are reported in parts per million (δ) deshield from TMS and coupling constant (J) are indicated in (Hz) Hertz. Hydrogen signal splitting templates are indicated for the multiplicities: *s*: singlet, *d*: doublet, *t*: triplet, *q*: quartet, *dd*: doublet of doublet, *m*: multiplet, and *br*: broad, signal for proton spectra.

2. Preparation of starting materials used in the synthesis of benzimidazole derivatives:

2.1. General procedure for synthesis of 1,4-bis(*p*-tolyloxy) butane:

A 25 mL round-bottom flask included *N,N*-dimethylformamide (DMF) (15 mL), *p*-cresol (5 mmol, 0.54 g), 1,4-dibromobutane (2.5 mmol, 0.3 mL), and potassium carbonate (K₂CO₃) (10 mmol, 1.8 g) were launched and the resulting blend was stirred on the magnetic stirrer at 110 °C about 8 h. Then, the reaction blend was directly shed into ice water (30 mL) and the white resulting powder was isolated. The obtained powder was washed with ethyl alcohol (EtOH) to achieve the pure desired compound².

2.1.1. 1,4-bis(*p*-tolyloxy) butane:

White powder; M.P. 104-106 °C; FT-IR (KBr, cm⁻¹): 2875-3033 (*br.* -CH₃ and -CH₂-), 1607 (C-O ether linkage); ¹H NMR (400 MHz, DMSO-*d*₆) δ 7.08 (d, *J* = 7.6 Hz, 4H), 6.82 (d, *J* = 7.9 Hz, 4H), 4.08 – 3.88 (m, 4H), 2.23 (s, 6H), 1.92 – 1.71 (m, 4H); ¹³C NMR (101 MHz, DMSO-*d*₆) δ 156.44, 129.74, 128.96, 114.22, 67.00, 25.45, 20.04.

2.2. General procedure for synthesis of 2,4,6-tris(*p*-tolyloxy)-1,3,5-triazine:

p-Cresol (3.0 mmol) was set into a round-bottom flask (100 mL), and 30 mL water and solid sodium hydroxide NaOH (3.0 mmol) was then added. A solution of cyanuric chloride (1.0 mmol) in 30 mL acetone was prepared and added dropwise into a solution of the *p*-cresol, then the resulting solution was stirred at room temperature for 3 h. The reaction blend was separated after completion which was checked with TLC and the resulting white powder was washed with acetone and water and then recrystallized from ethanol to obtain triazine-based tris-toluene³.

2.2.1. 2,4,6-tris(*p*-tolyloxy)-1,3,5-triazine:

White powder; M.P. 213-215 °C; FT-IR (KBr, cm⁻¹): 3041-3067 (*br.* -CH₃), 1577 (C-O ether linkage); ¹H NMR (400 MHz, DMSO-*d*₆) δ 7.22 (d, *J* = 7.7 Hz, 6H), 7.10 (d, *J* = 7.8 Hz, 6H), 2.31 (s, 9H); ¹³C NMR (101 MHz, DMSO-*d*₆) δ 173.13, 149.17, 135.16, 129.82, 121.10, 20.36.

2.3. NMR (¹H and ¹³C) and FT-IR data of synthesized benzimidazole:

2.3.1. 2-phenyl-1*H*-benzo[*d*]imidazole (3a):

Light yellow powder; M.P. >300 °C; FT-IR (KBr, cm⁻¹): 3420 (*br.* NH benzimidazole), 1577 (C=N benzimidazole); ¹H NMR (400 MHz, DMSO-*d*₆) δ 8.41 (dd, *J* = 7.7, 1.9 Hz, 2H), 7.86 (dd, *J* = 6.1, 3.1 Hz, 2H), 7.75 – 7.73 (m, 2H), 7.57 (dd, *J* = 6.1, 3.1 Hz, 2H), 7.04 (s, 1H); ¹³C NMR (101 MHz, DMSO-*d*₆) δ 148.66, 133.23, 131.98, 129.59, 128.06, 125.82, 123.30, 114.00.

2.3.2. 2-(4-chlorophenyl)-1*H*-benzo[*d*]imidazole (3b):

Light brown powder; M.P. >300 °C; FT-IR (KBr, cm⁻¹): 3438 (*br.* NH benzimidazole), 1578 (C=N benzimidazole); ¹H NMR (400 MHz, DMSO-*d*₆) δ 8.43 (d, *J* = 8.6 Hz, 2H), 7.86 (d, *J* = 3.2 Hz, 1H), 7.83 (d, *J* = 8.3 Hz, 3H), 7.56 (dd, *J* = 6.1, 3.1 Hz, 2H); ¹³C NMR (101 MHz, DMSO-*d*₆) δ 147.73, 137.91, 132.26, 129.79, 129.70, 125.79, 122.56.

2.3.3. 2-(4-nitrophenyl)-1*H*-benzo[*d*]imidazole (3c):

Brown powder; M.P. >300 °C; FT-IR (KBr, cm⁻¹): 3449 (*br.* NH benzimidazole), 1605 (C=N benzimidazole); ¹H NMR (400 MHz, DMSO-*d*₆) δ 8.65 (d, *J* = 8.8 Hz, 2H), 8.50 (d, *J* = 8.8 Hz, 2H), 7.86 (dd, *J* = 6.1, 3.1 Hz, 2H), 7.55 (dd, *J* = 6.1, 3.1 Hz, 2H); ¹³C NMR (101 MHz, DMSO-*d*₆) δ 149.31, 146.65, 133.03, 129.92, 129.25, 125.95, 124.44, 114.42.

2.3.4. 5-nitro-2-(4-nitrophenyl)-1*H*-benzo[*d*]imidazole (3d):

Dark brown powder; M.P. >300 °C; FT-IR (KBr, cm⁻¹): 3344 (*br.* NH benzimidazole), 1578 (C=N benzimidazole); ¹H NMR (400 MHz, DMSO-*d*₆) δ 8.46 (d, *J* = 1.8 Hz, 1H), 8.42 – 8.35 (m, 4H), 8.11 (dd, *J* =

8.9, 2.0 Hz, 1H), 7.77 (d, J = 8.9 Hz, 1H); ^{13}C NMR (101 MHz, DMSO- d_6) δ 153.26, 148.33, 143.05, 134.57, 127.99, 124.22, 118.46, 112.74.

2.3.5. 4-(1*H*-benzo[*d*]imidazol-2-yl)-N, N-dimethylaniline (3e):

Yellow powder; M.P. 230-232 °C; FT-IR (KBr, cm⁻¹): 3425 (*br.* NH benzimidazole), 1605 (C=N benzimidazole); ^1H NMR (400 MHz, DMSO- d_6) δ 15.27 (s, 1H), 8.26 (d, J = 9.1 Hz, 2H), 7.73 (dd, J = 6.1, 3.2 Hz, 2H), 7.46 (dd, J = 6.1, 3.1 Hz, 2H), 6.87 (d, J = 9.1 Hz, 2H), 3.04 (s, 6H); ^{13}C NMR (101 MHz, DMSO- d_6) δ 153.08, 149.26, 131.37, 129.49, 125.04, 113.02, 111.65, 107.81, 39.54.

2.3.6. N, N-dimethyl-4-(5-nitro-1*H*-benzo[*d*]imidazol-2-yl) aniline (3f):

Yellow powder; M.P. 281-283 °C; FT-IR (KBr, cm⁻¹): 3425 (*br.* NH benzimidazole), 1581 (C=N benzimidazole); ^1H NMR (400 MHz, DMSO- d_6) δ 8.41 (d, J = 1.8 Hz, 1H), 8.27 (dd, J = 8.9, 2.0 Hz, 1H), 8.19 (d, J = 9.0 Hz, 2H), 7.84 (d, J = 8.9 Hz, 1H), 6.92 (d, J = 9.0 Hz, 2H), 3.08 (s, 6H); ^{13}C NMR (101 MHz, DMSO- d_6) δ 153.80, 153.31, 143.77, 137.72, 133.04, 129.69, 119.98, 113.67, 111.82, 109.25.

2.3.7. 2-(4-methoxyphenyl)-1*H*-benzo[*d*]imidazole (3g):

White powder; M.P. 259-261 °C; FT-IR (KBr, cm⁻¹): 3422 (*br.* NH benzimidazole), 1578 (C=N benzimidazole); ^1H NMR (400 MHz, DMSO- d_6) δ 8.38 (d, J = 8.9 Hz, 2H), 7.82 (dd, J = 6.1, 3.1 Hz, 2H), 7.54 (dd, J = 6.1, 3.1 Hz, 2H), 7.29 (d, J = 8.9 Hz, 2H), 3.91 (s, 3H); ^{13}C NMR (101 MHz, DMSO- d_6) δ 163.14, 148.73, 131.78, 130.07, 125.54, 115.15, 113.66, 55.79.

2.3.8. 2-(4-methoxyphenyl)-5-nitro-1*H*-benzo[*d*]imidazole (3h):

Cream powder; M.P. > 300 °C; FT-IR (KBr, cm⁻¹): 3432 (*br.* NH benzimidazole), 1605 (C=N benzimidazole); ^1H NMR (400 MHz, DMSO- d_6) δ 8.48 (d, J = 2.1 Hz, 1H), 8.33 (d, J = 8.8 Hz, 2H), 8.26 (dd, J = 8.9, 2.1 Hz, 1H), 7.88 (d, J = 8.9 Hz, 1H), 7.24 (d, J = 8.9 Hz, 2H), 3.89 (s, 3H); ^{13}C NMR (101 MHz, DMSO- d_6) δ 162.86, 153.88, 143.69, 139.09, 134.71, 129.89, 119.59, 117.28, 114.97, 114.40, 110.44, 55.70.

2.3.9. (2-(4-chlorophenyl)-1*H*-benzo[*d*]imidazol-6-yl) (phenyl)methanone (3i):

Yellow powder; M.P. > 300 °C; FT-IR (KBr, cm⁻¹): 3448 (*br.* NH benzimidazole), 1610 (C=N benzimidazole); ^1H NMR (400 MHz, DMSO- d_6) δ 8.31 (d, J = 8.6 Hz, 2H), 8.02 (s, 1H), 7.84 (d, J = 8.5 Hz, 1H), 7.80 – 7.75 (m, 3H), 7.71 (dd, J = 15.4, 8.1 Hz, 3H), 7.59 (t, J = 7.6 Hz, 2H); ^{13}C NMR (101 MHz, DMSO- d_6) δ 195.16, 151.65, 139.30, 137.55, 136.53, 136.05, 132.40, 129.51, 129.42, 129.08, 128.48, 125.77, 125.49, 117.26, 114.63.

2.3.10. (2-(4-nitrophenyl)-1*H*-benzo[*d*]imidazol-5-yl) (phenyl)methanone (3j):

Yellow powder; M.P. > 300 °C; FT-IR (KBr, cm⁻¹): 3448 (*br.* NH benzimidazole), 1610 (C=N benzimidazole); ^1H NMR (400 MHz, DMSO- d_6) δ 8.52 – 8.41 (m, 4H), 8.02 (s, 1H), 7.86 – 7.74 (m, 4H), 7.73 – 7.66 (m, 1H), 7.63 – 7.56 (m, 2H); ^{13}C NMR (101 MHz, DMSO- d_6) δ 195.32, 151.10, 148.39, 137.67, 134.15, 132.31, 132.12, 129.50, 128.91, 128.46, 128.36, 128.10, 125.19, 124.34, 115.14.

2.3.11. 1,3-dihydrospiro[benzo[*d*]imidazole-2,9'-fluorene] (3k):

Dark brown powder; 292-294 °C; FT-IR (KBr, cm⁻¹): 3408 (*br.* NH benzimidazole), 1577 (C=N benzimidazole); ^1H NMR (400 MHz, DMSO- d_6) δ 8.05 (dd, J = 6.2, 3.5 Hz, 2H), 7.73 (dd, J = 6.3, 3.3 Hz, 2H), 7.05 – 7.03 (m, 2H), 7.02 – 7.01 (m, 2H), 6.89 – 6.86 (m, 4H).

2.3.12. 1,4-bis(4-(1*H*-benzo[*d*]imidazol-2-yl) phenoxy) butane (3l):

Light brown powder; M.P. 187-189 °C; FT-IR (KBr, cm⁻¹): 3409 (*br.* NH benzimidazole), 1605 (C=N benzimidazole); ¹H NMR (400 MHz, DMSO-*d*₆) δ 8.54 – 8.40 (m, 2H), 7.91 – 7.80 (m, 3H), 7.56 – 7.45 (m, 2H), 7.30 – 7.18 (m, 3H), 7.15 – 7.06 (m, 3H), 6.96 – 6.85 (m, 3H), 4.23 – 3.91 (m, 4H), 1.97 – 1.78 (m, 4H); ¹³C NMR (101 MHz, DMSO-*d*₆) δ 162.59, 148.37, 131.43, 130.27, 128.13, 120.88, 115.47, 114.74, 113.56, 67.77, 25.09.

2.3.13. 6-nitro-2-(4-(4-(4-(5-nitro-1*H*-benzo[*d*]imidazol-2-yl)phenoxy)butoxy)phenyl)-1*H*-benzo[*d*]imidazole (3m):

Brown powder; M.P. 194-196 °C; FT-IR (KBr, cm⁻¹): 3434 (*br.* NH benzimidazole), 1579 (C=N benzimidazole); ¹H NMR (400 MHz, DMSO-*d*₆) δ 8.70 – 8.39 (m, 2H), 8.36 – 8.11 (m, 3H), 8.01 – 7.58 (m, 3H), 7.34 – 7.11 (m, 3H), 7.04 – 6.72 (m, 3H), 4.21 – 3.93 (m, 4H), 1.93 – 1.77 (m, 4H); ¹³C NMR (101 MHz, DMSO-*d*₆) δ 162.24, 158.11, 153.69, 143.65, 134.51, 131.11, 131.08, 129.91, 129.01, 127.60, 127.37, 119.59, 116.94, 115.30, 114.97, 114.76, 114.27, 110.34, 67.68, 66.99, 25.14, 18.51.

2.3.14. 2,4,6-tris(4-(1*H*-benzo[*d*]imidazol-2-yl) phenoxy)-1,3,5-triazine (3n):

Yellow powder; M.P. >300 °C; FT-IR (KBr, cm⁻¹): 3437 (*br.* NH benzimidazole), 1578 (C=N benzimidazole); ¹H NMR (400 MHz, DMSO-*d*₆) δ 8.44 (d, *J* = 12.1, 9.0 Hz, 6H), 7.74 (dd, *J* = 6.1, 3.2 Hz, 6H), 7.61 (d, *J* = 21.6, 9.6 Hz, 6H), 7.43 (dd, *J* = 6.1, 3.1 Hz, 6H); ¹³C NMR (101 MHz, DMSO-*d*₆) δ 172.80, 153.91, 148.47, 133.98, 129.19, 124.74, 122.60, 114.21.

3. General procedure for preparation modified with g-C₃N₄ and Fe^{III}/g-C₃N₄ and unmodified CPEs:

Firstly, the carbon paste electrode (CPE) was produced by hand blending graphite powder and mineral oil in a ratio of 12 mg:6 mg for 1 hour in an agate pounder to get a carbon paste. The achieved CPE was filled into the homemade Teflon cavity and electrical contact was provided by copper wire at the end of the PVC tube. The surface of CPEs was cleaned by rubbing their outer surface on a piece of paper before use. The modified CPEs with g-C₃N₄ and Fe-C₃N₄ were produced in the same method, 2mg g-C₃N₄ and nanocomposite Fe-C₃N₄ were added to the graphite powder (12mg) and mineral oil (6mg) in the initial step.

3.1. Photoelectrochemical measurements

The photocurrent was run on an electrochemical instrument in a standard three-electrode with a Pt wire as the working electrode, FTO as the counter electrode and Ag/AgCl (sutured KCl) as a reference electrode. A Xe arc lamp *via* a UV-separator filter ($\lambda > 400$ nm) was used as a light source with an intensity of 0.6 V applied potential. Na₂SO₄ (0.5 M) aqueous solution was used as the electrolyte.

EDX and elemental analysis investigation nanocomposite Fe^{III}/g-C₃N₄ (0.02 wt%):

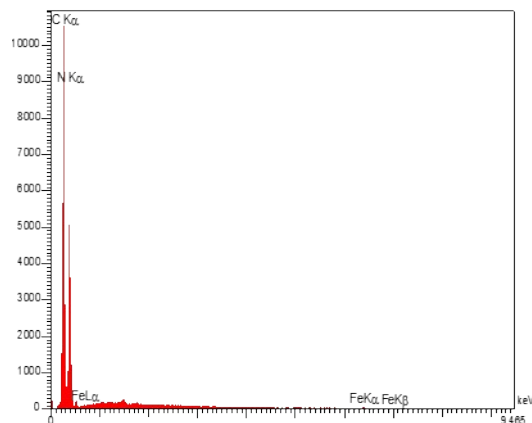


Figure S2. EDX of) Fe^{III}/g-C₃N₄ (0.02wt%)

Table S1. Percentage weight of elements and atoms obtained from EDX analysis for nanocomposite Fe^{III}/g-C₃N₄ (0.02 wt%)

Elt	Line	Int	W%	A%
C	Ka	797.1	30.26	33.61
N	Ka	399.6	69.72	66.39
Fe	Ka	1.8	0.02	0.01
		100.00	100.00	

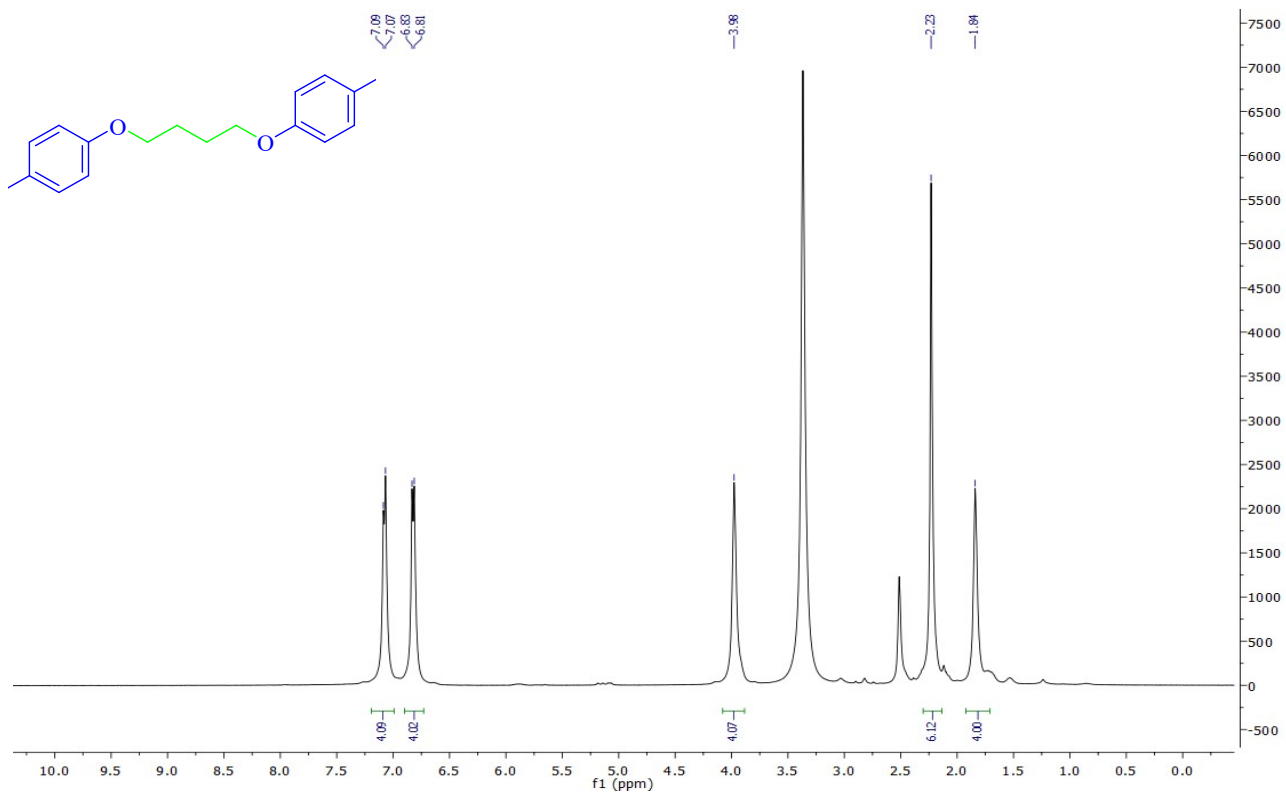


Figure S3. ^1H NMR of 1,4-bis(*p*-tolyloxy) butane in $\text{DMSO}-d_6$

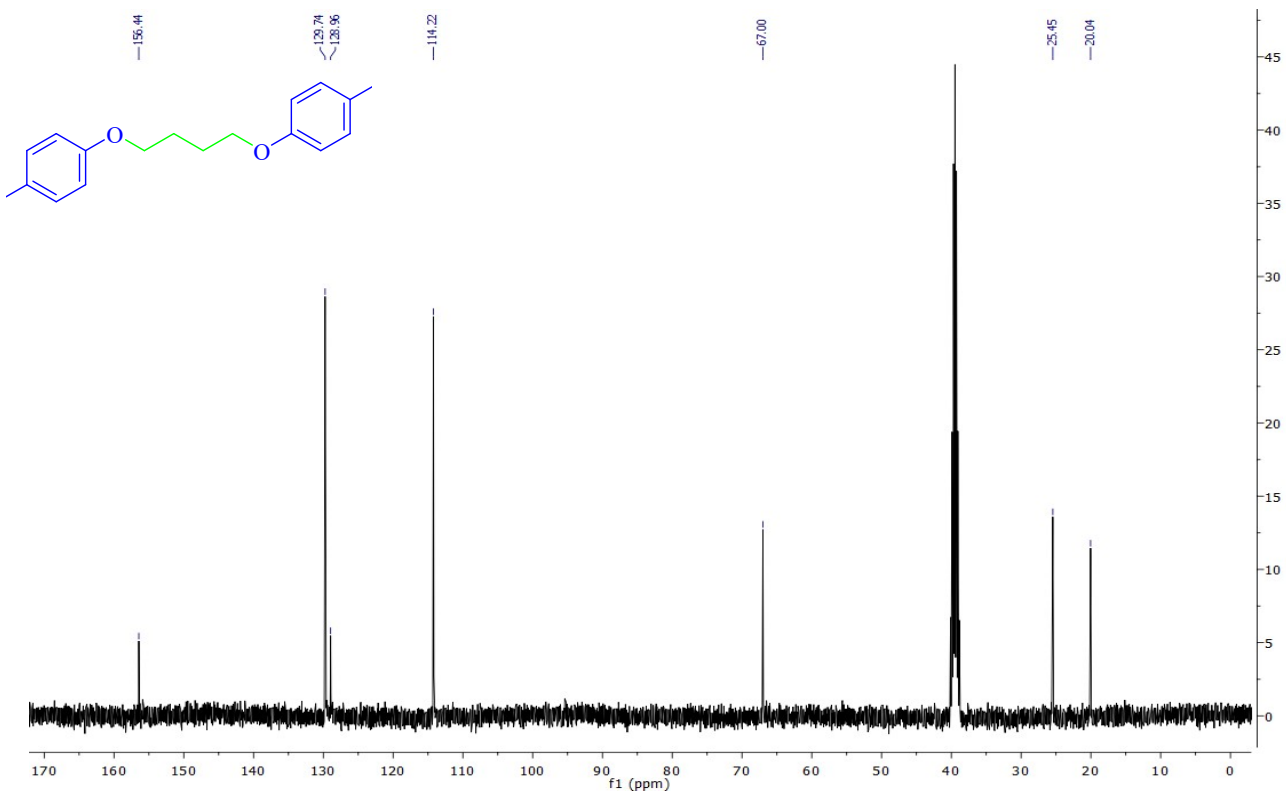


Figure S4. ^{13}C NMR of 1,4-bis(*p*-tolyloxy) butane in $\text{DMSO}-d_6$

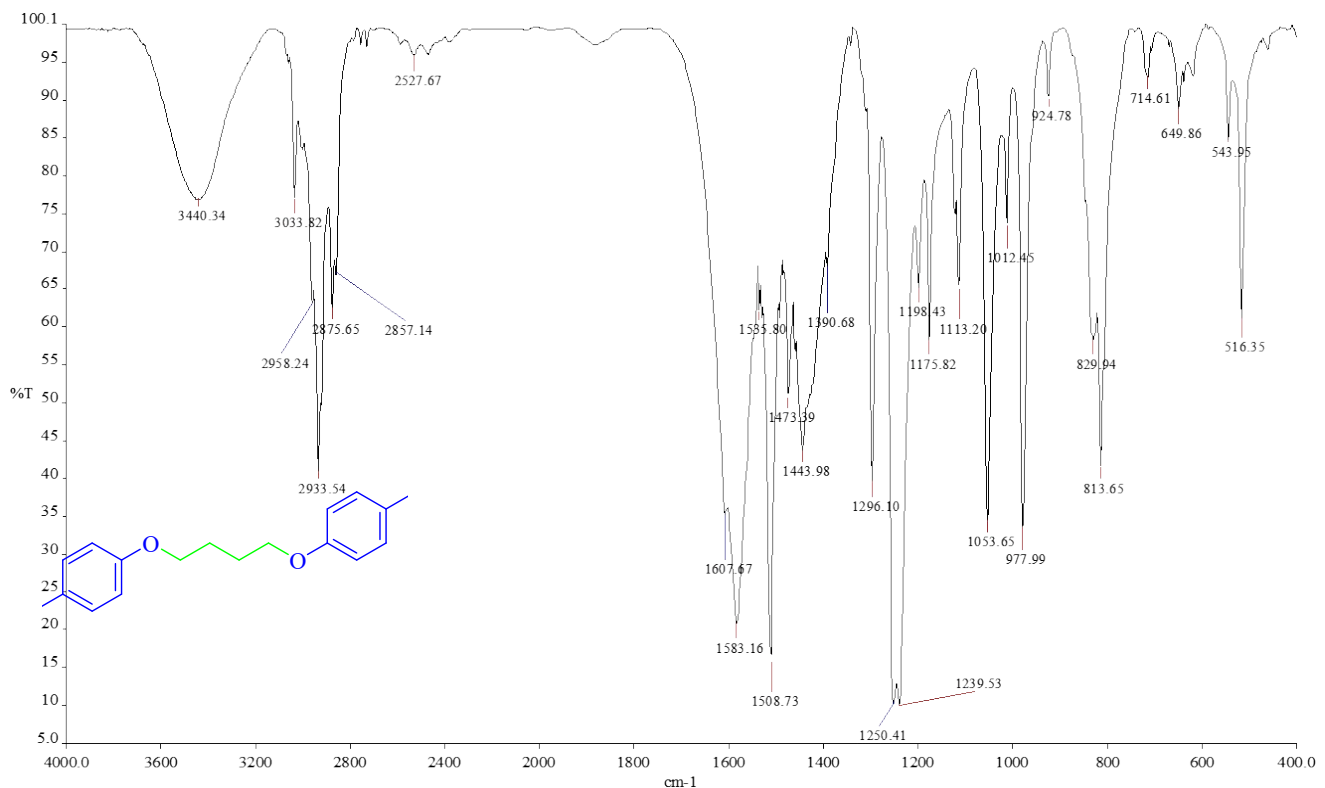
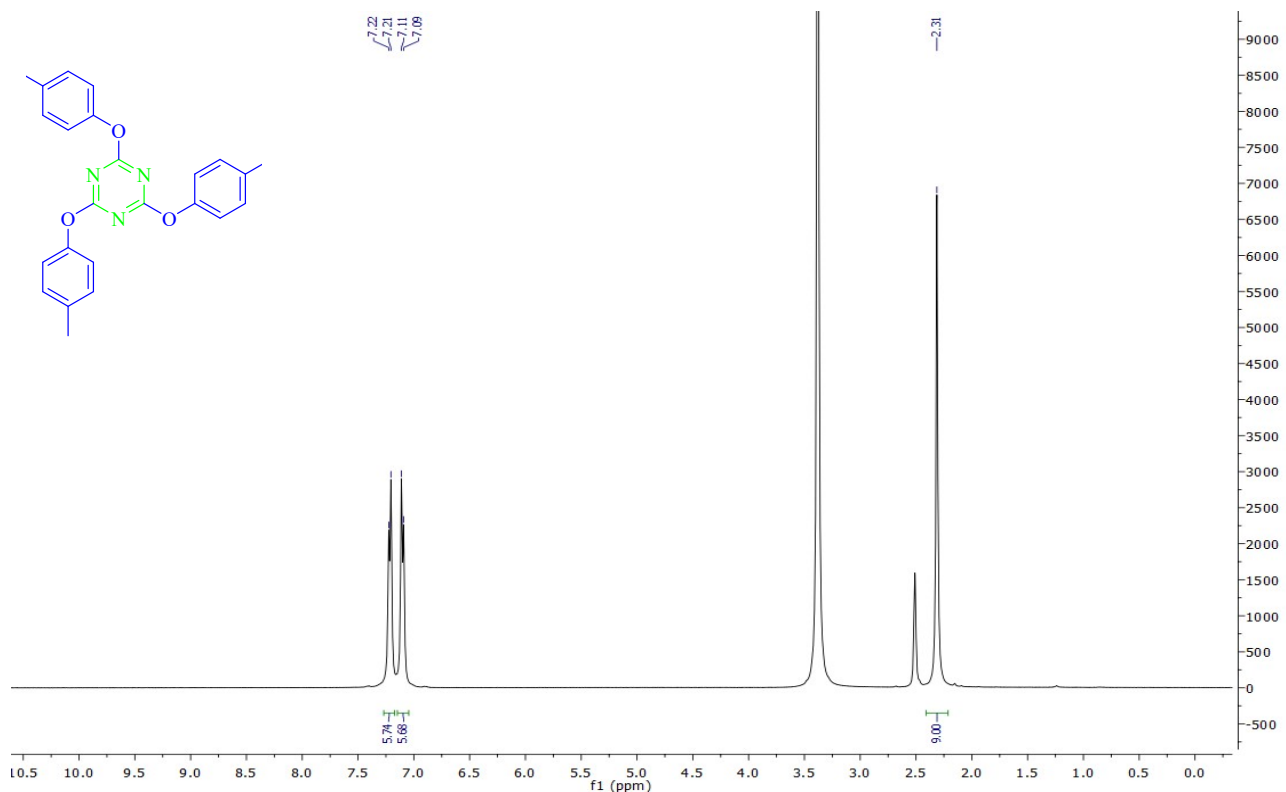


Figure S5. FT-IR spectrum of 1,4-bis(*p*-tolyloxy) butane with KBr pellet



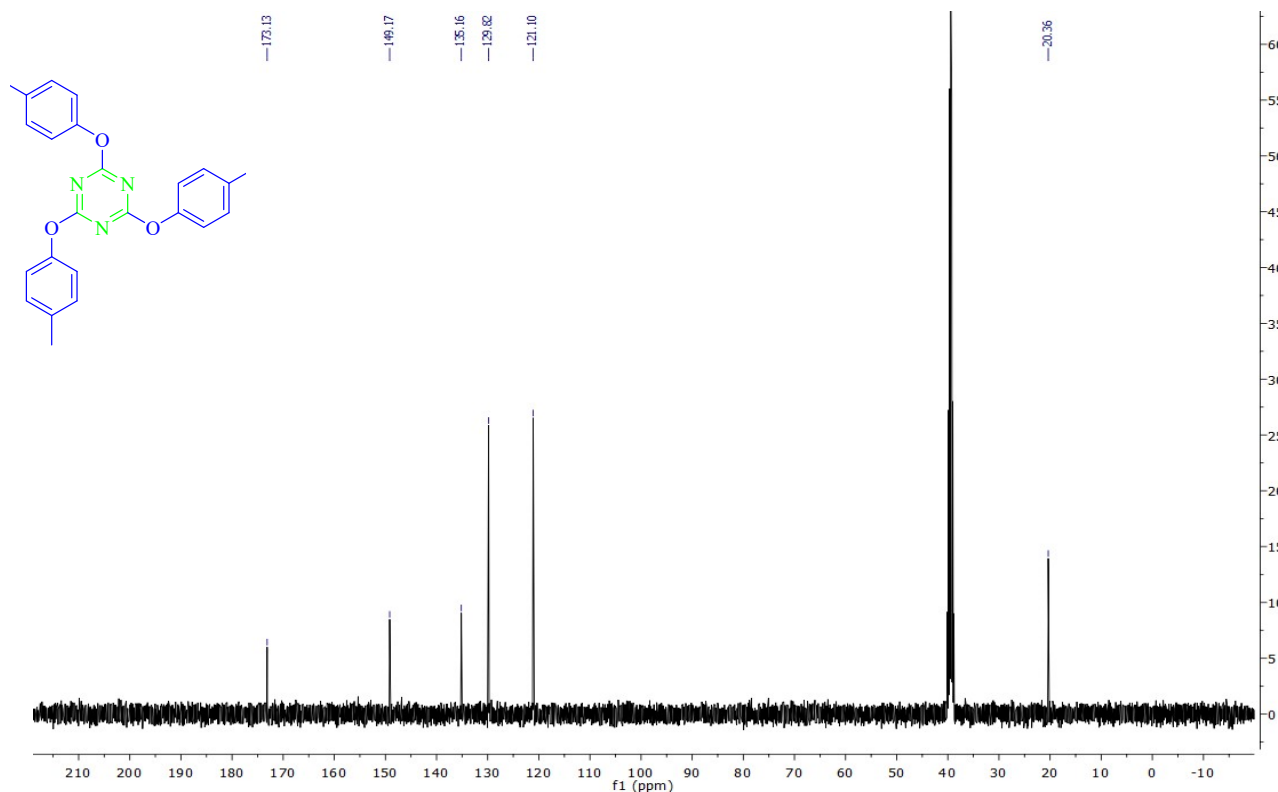


Figure S7. ^{13}C NMR of 2,4,6-tris(*p*-tolyloxy)-1,3,5-triazine in $\text{DMSO}-d_6$

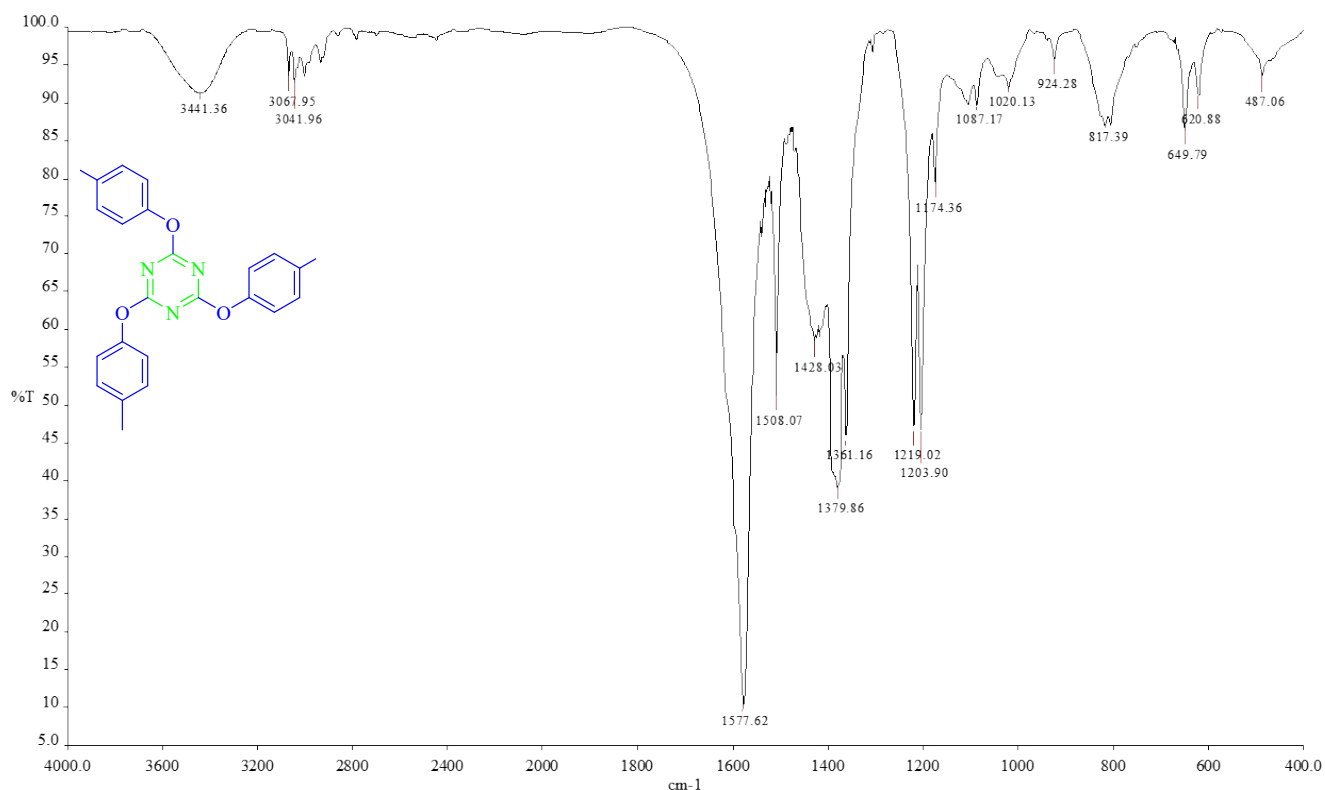


Figure S8. FT-IR spectrum of 2,4,6-tris(*p*-tolyloxy)-1,3,5-triazine with KBr pellet

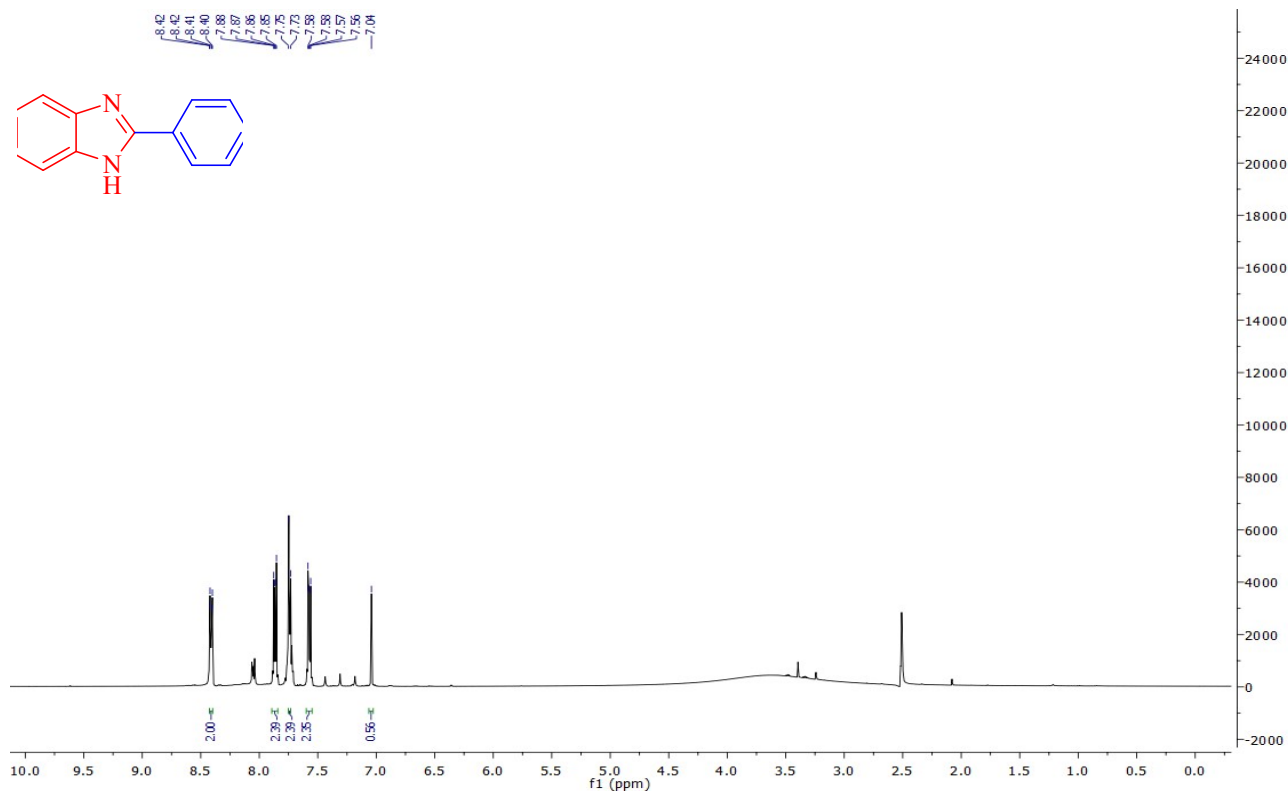


Figure S9. ^1H NMR of 2-phenyl-1*H*-benzo[*d*]imidazole (**3a**) in $\text{DMSO}-d_6$

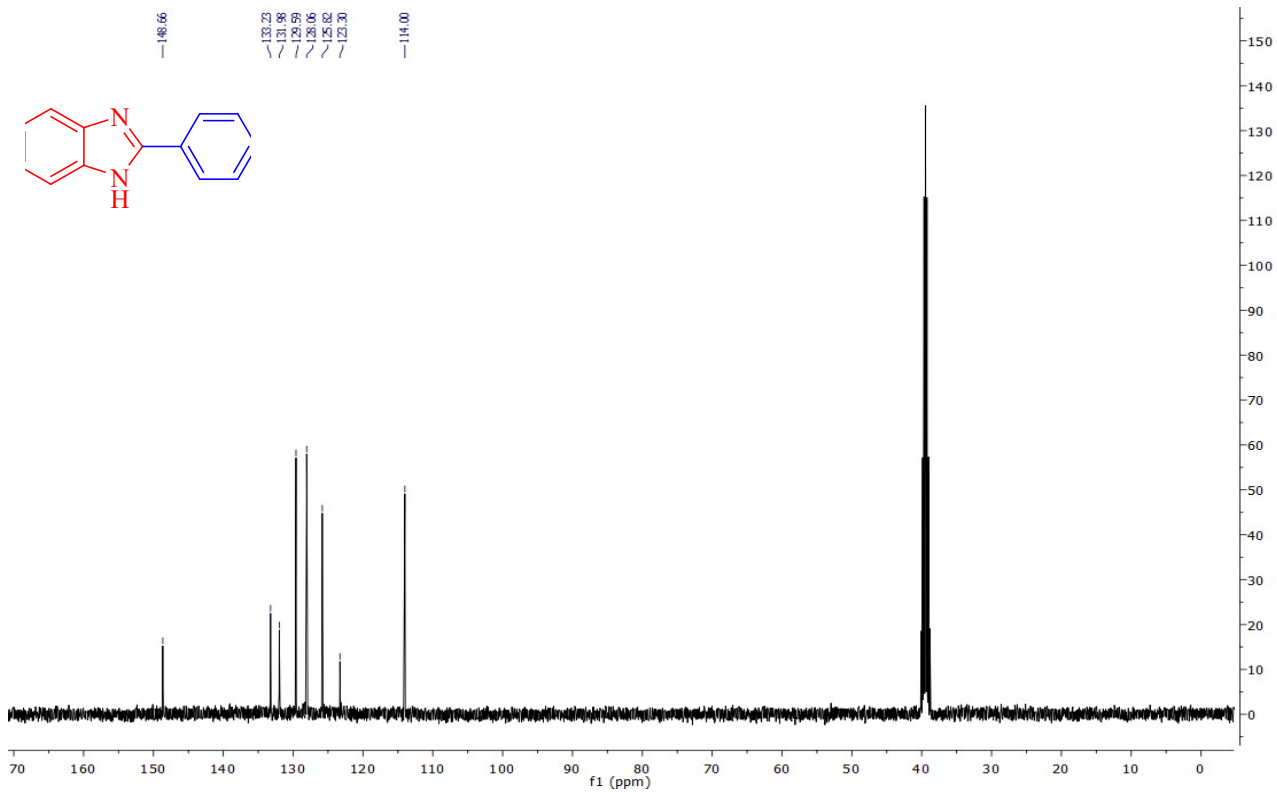


Figure S10. ^{13}C NMR of 2-phenyl-1*H*-benzo[*d*]imidazole (**3a**) in $\text{DMSO}-d_6$

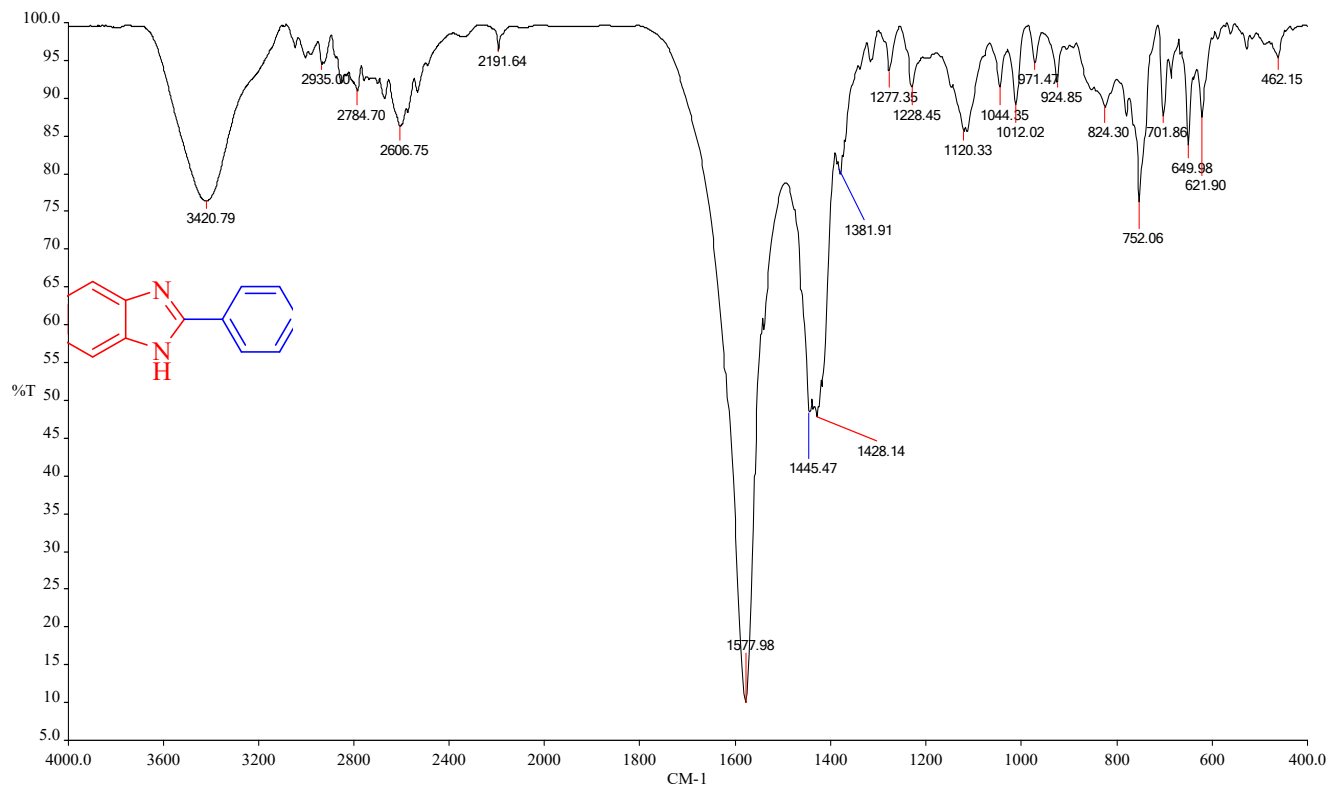
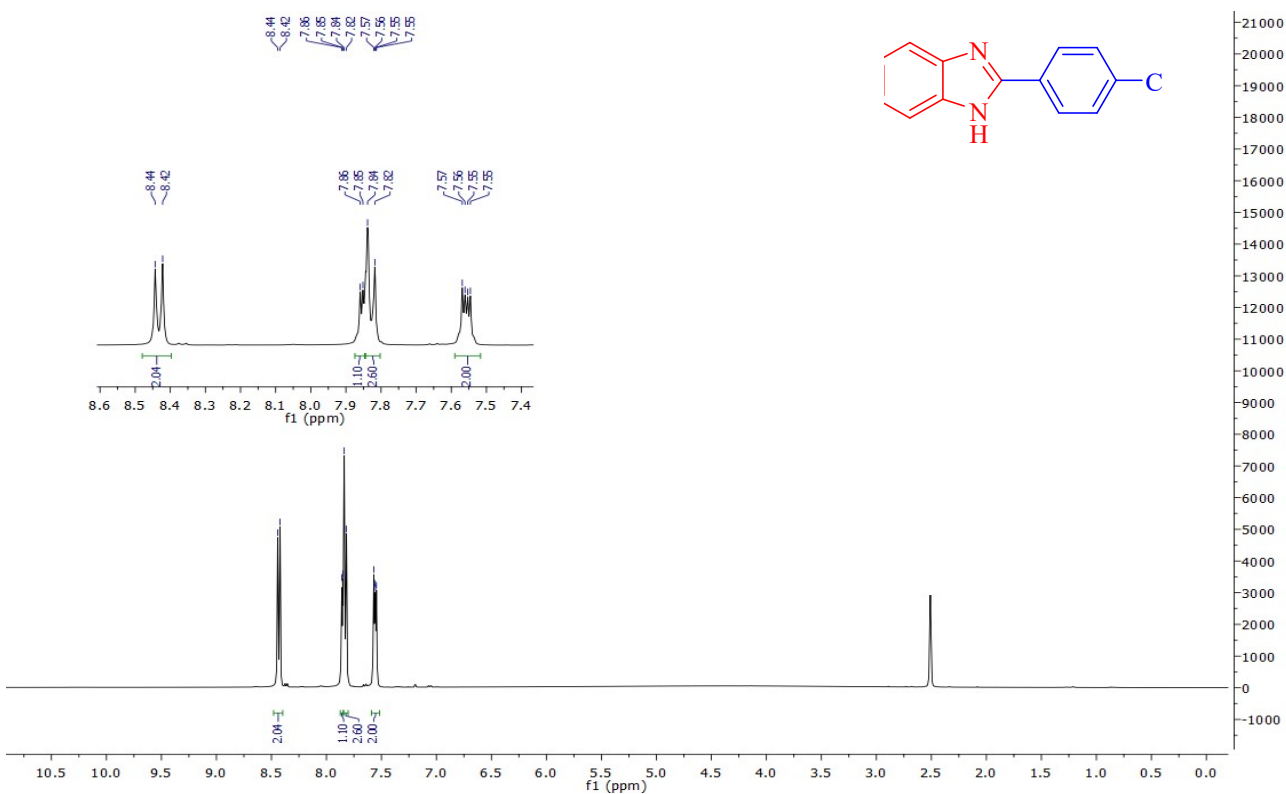


Figure S11. FT-IR spectrum of 2-phenyl-1*H*-benzo[*d*]imidazole (**3a**) with KBr pellet



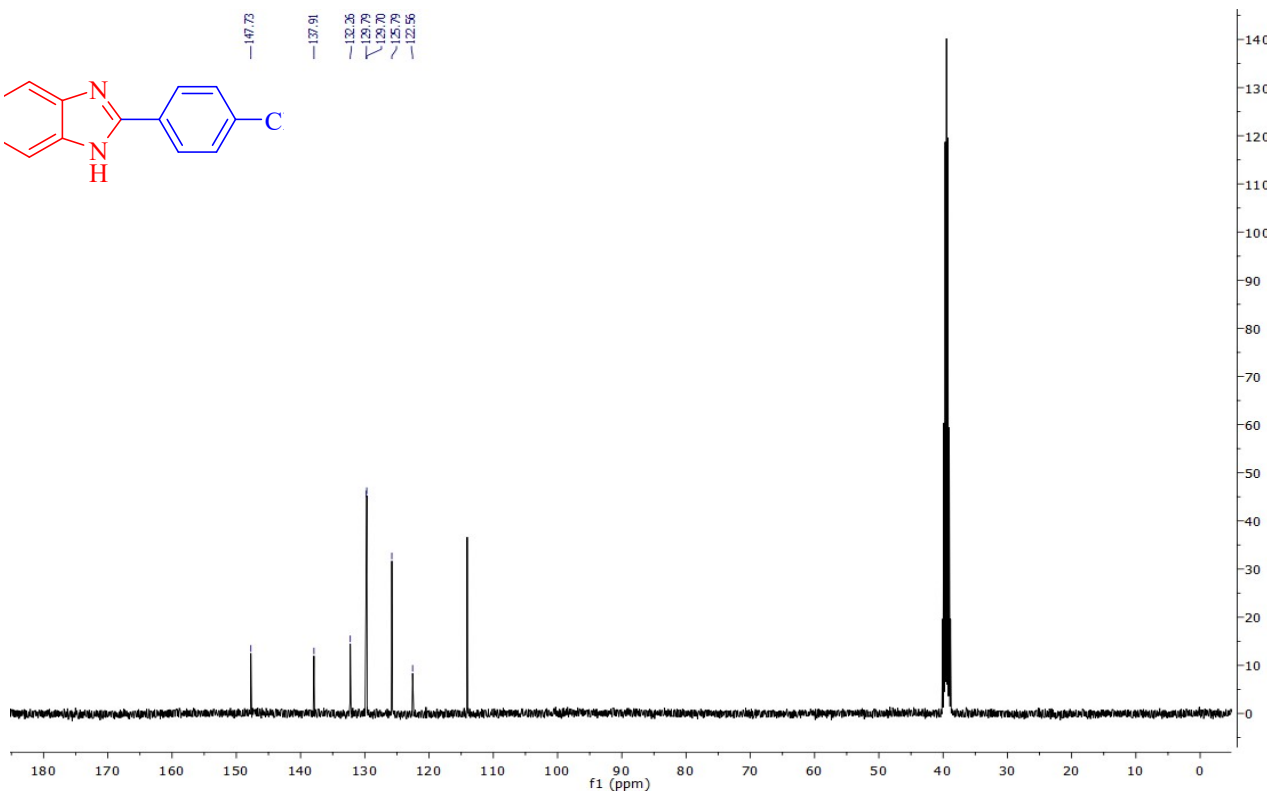


Figure S13. ^{13}C NMR of 2-(4-chlorophenyl)-1*H*-benzo[*d*]imidazole (**3b**) in $\text{DMSO}-d_6$

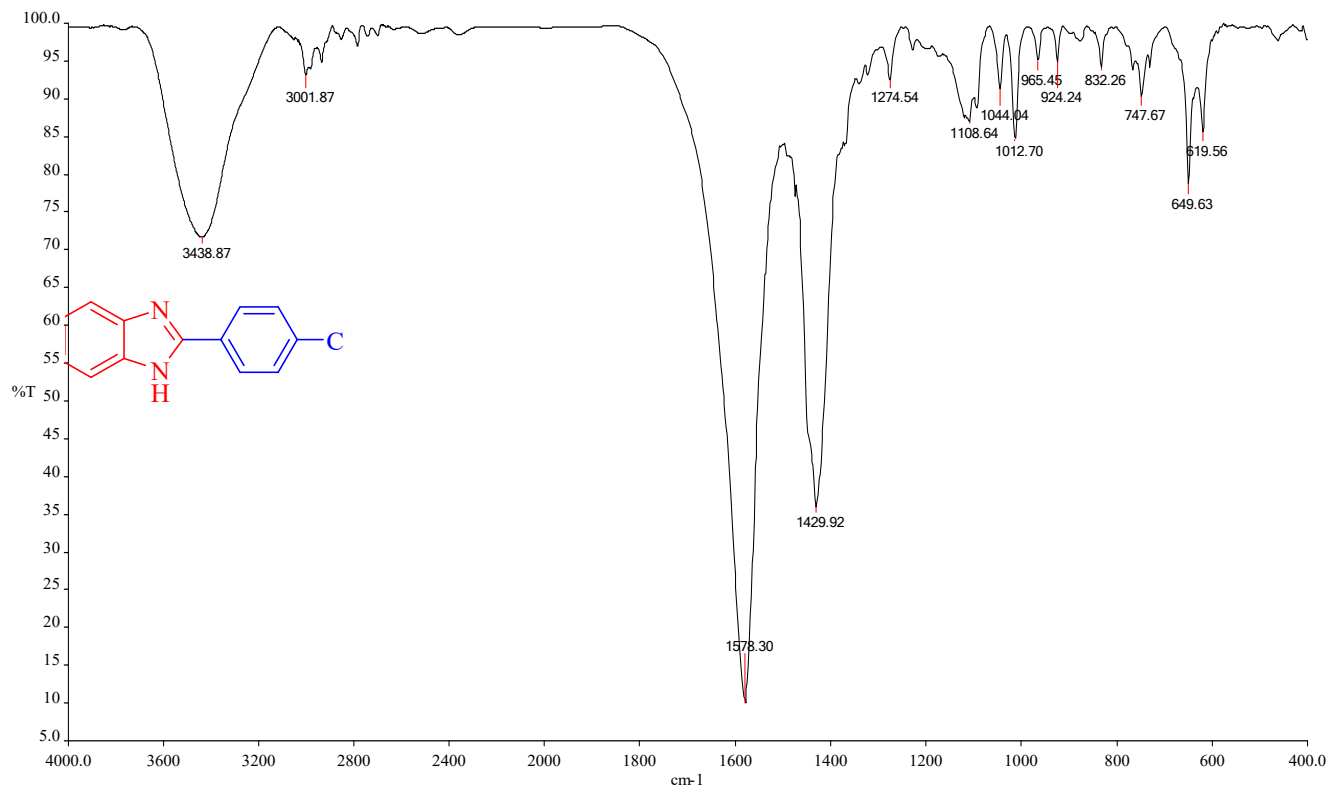


Figure S14. FT-IR spectrum of 2-(4-chlorophenyl)-1*H*-benzo[*d*]imidazole (**3b**) with KBr pellet

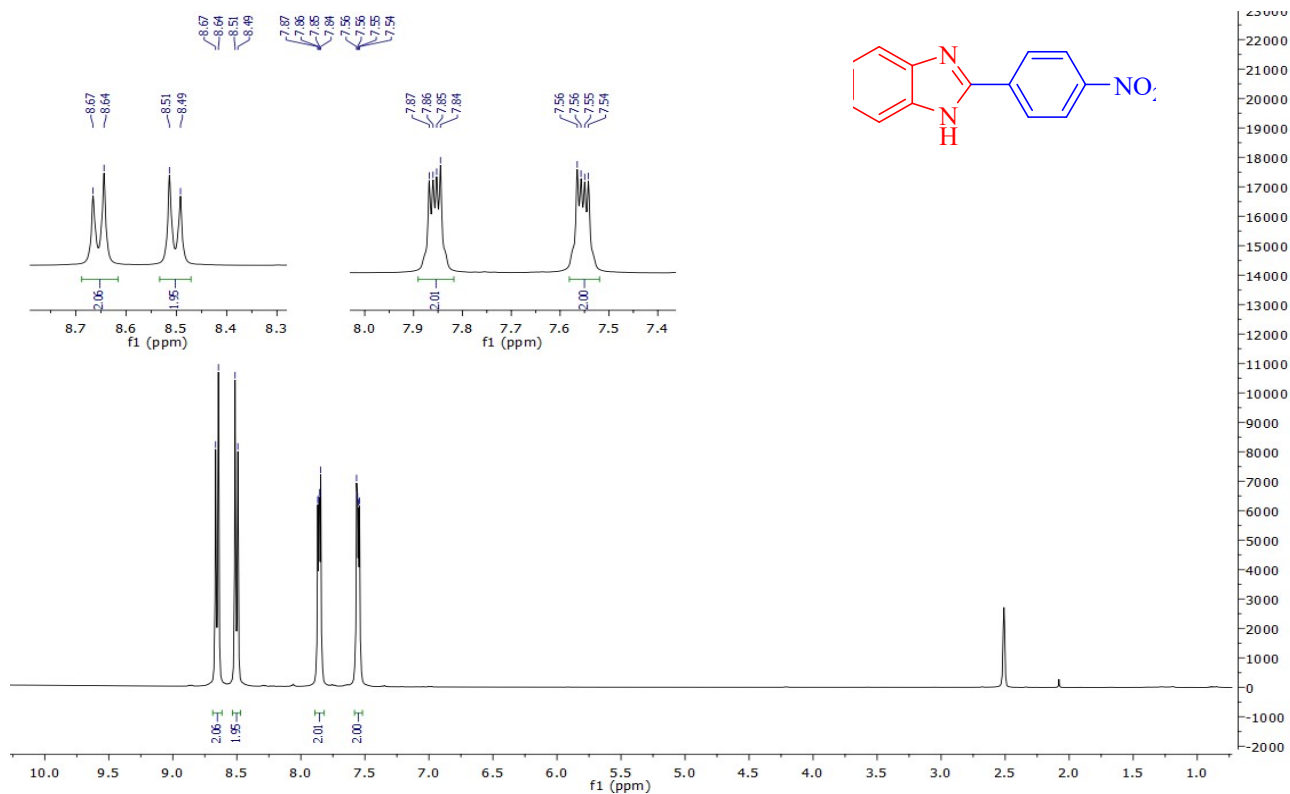


Figure S15. ^1H NMR of 2-(4-nitrophenyl)-1*H*-benzo[*d*]imidazole (**3c**) in $\text{DMSO}-d_6$

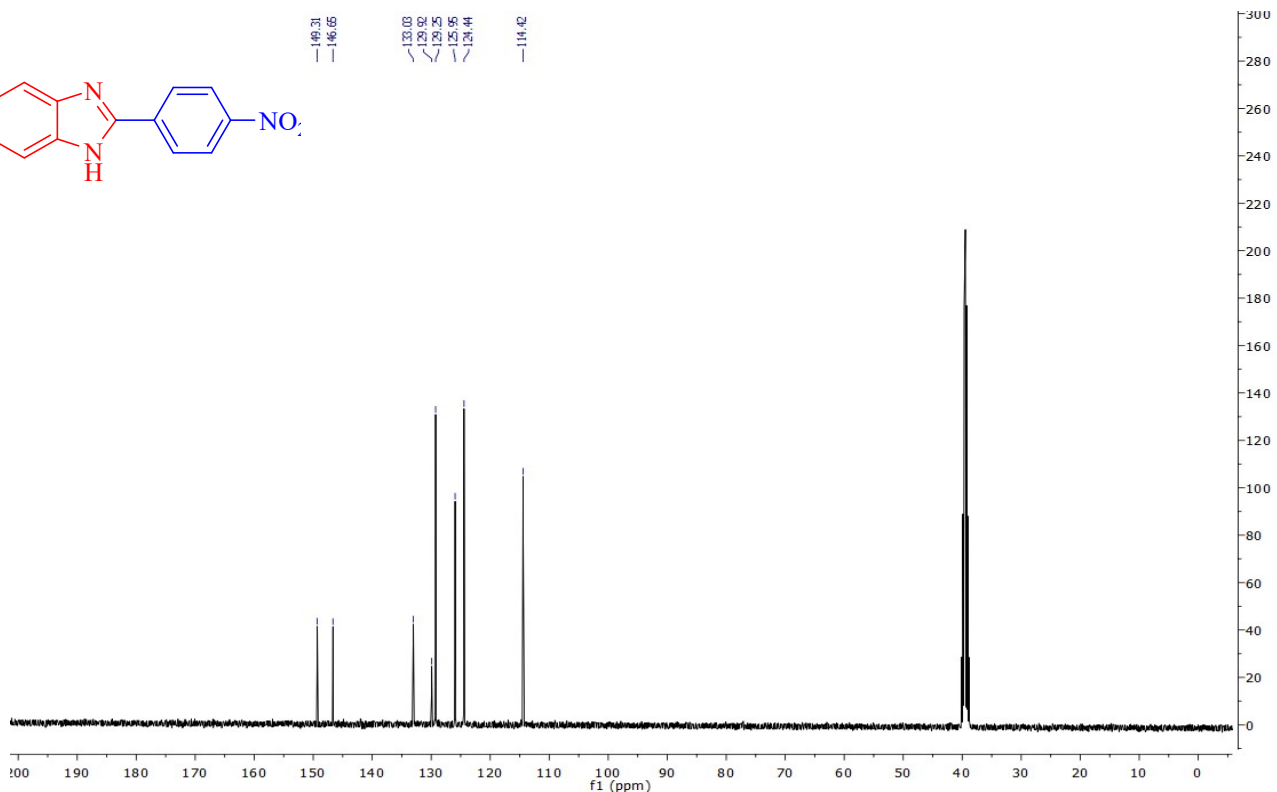


Figure S16. ^{13}C NMR of 2-(4-nitrophenyl)-1*H*-benzo[*d*]imidazole (**3c**) in $\text{DMSO}-d_6$

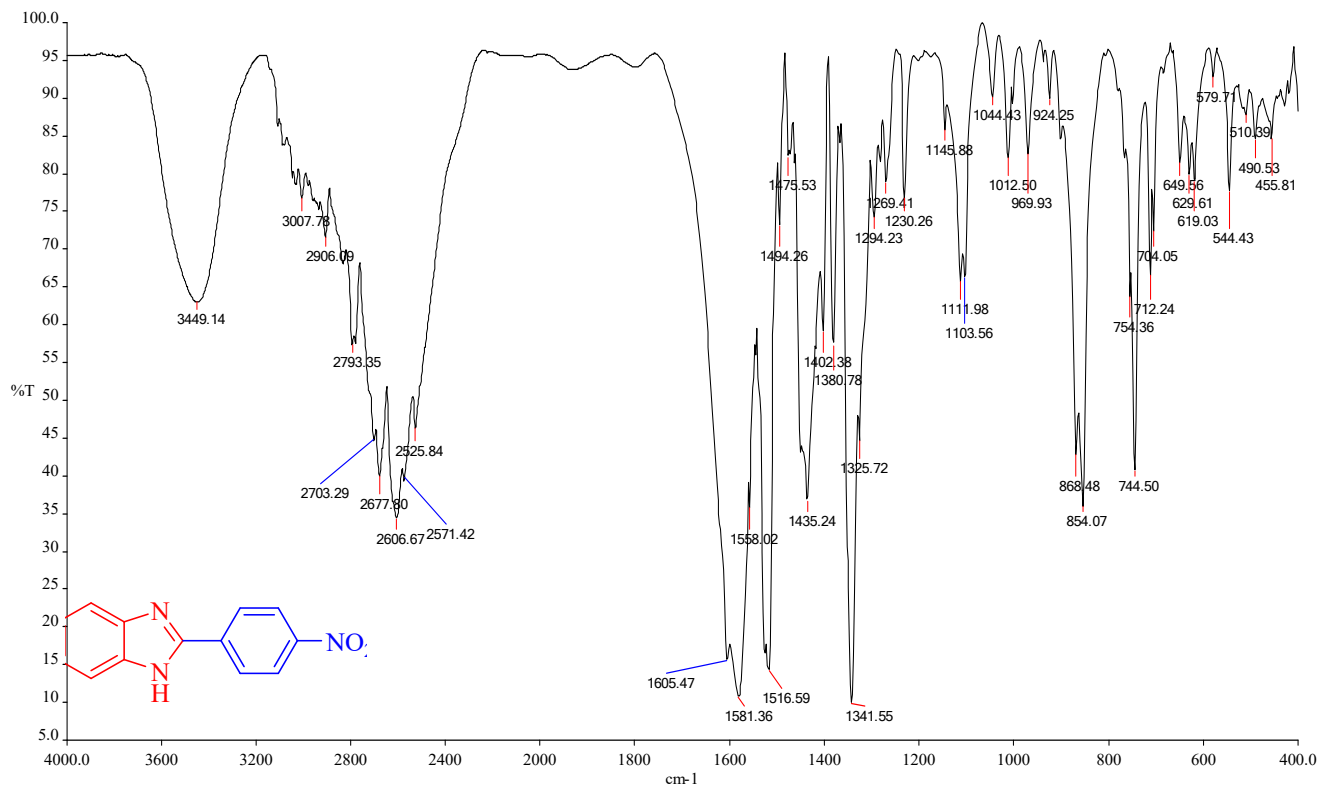


Figure S17. FT-IR spectrum of 2-(4-nitrophenyl)-1*H*-benzo[*d*]imidazole (**3c**) with KBr pellet

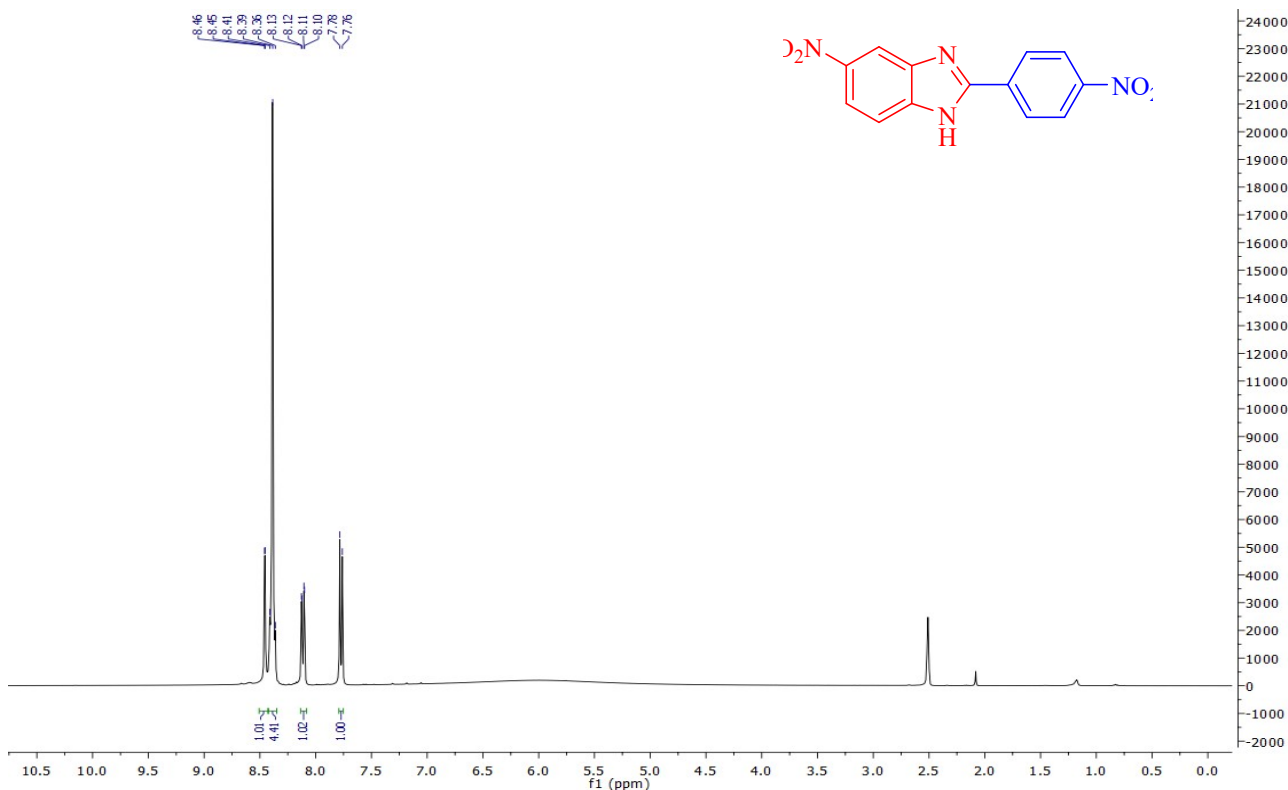


Figure S18. ^1H NMR of 5-nitro-2-(4-nitrophenyl)-1*H*-benzo[*d*]imidazole (**3c**) in $\text{DMSO}-d_6$

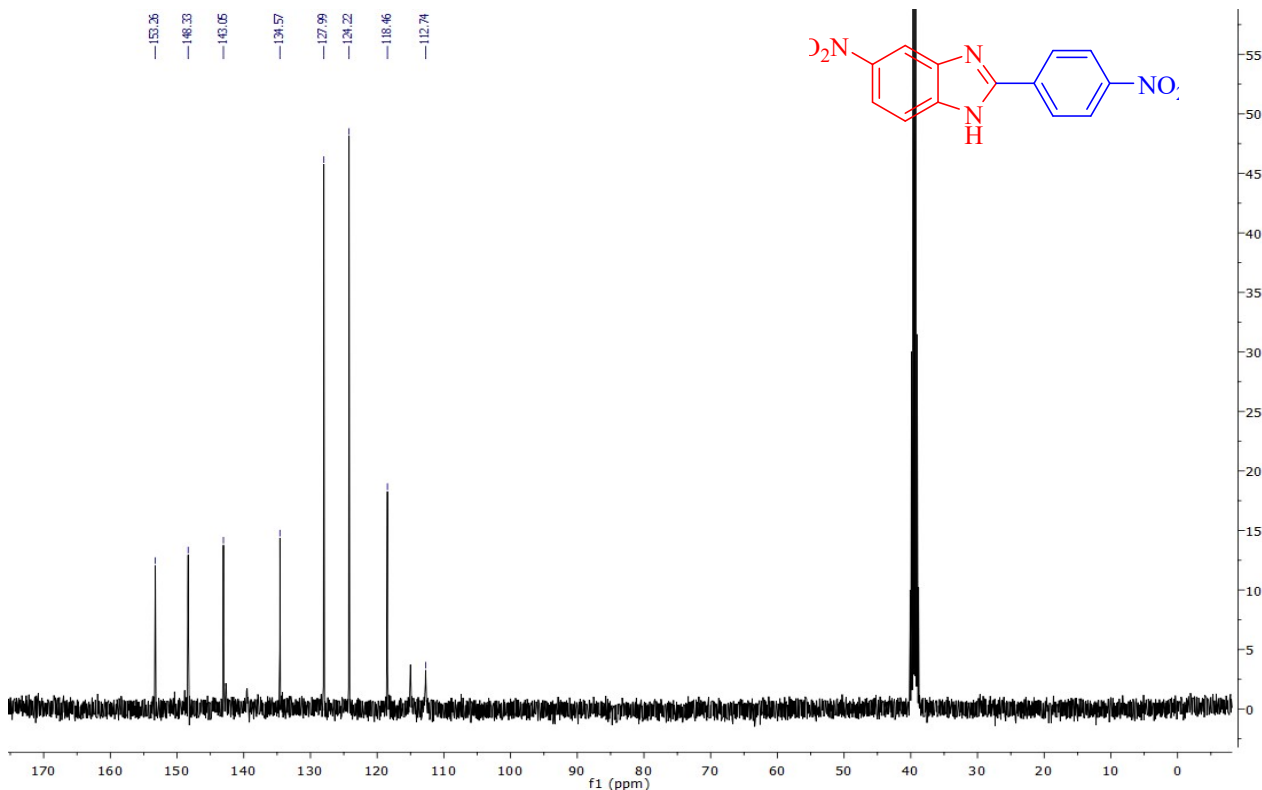


Figure S19. ^{13}C NMR of 5-nitro-2-(4-nitrophenyl)-1*H*-benzo[*d*]imidazole (**3d**) in $\text{DMSO}-d_6$

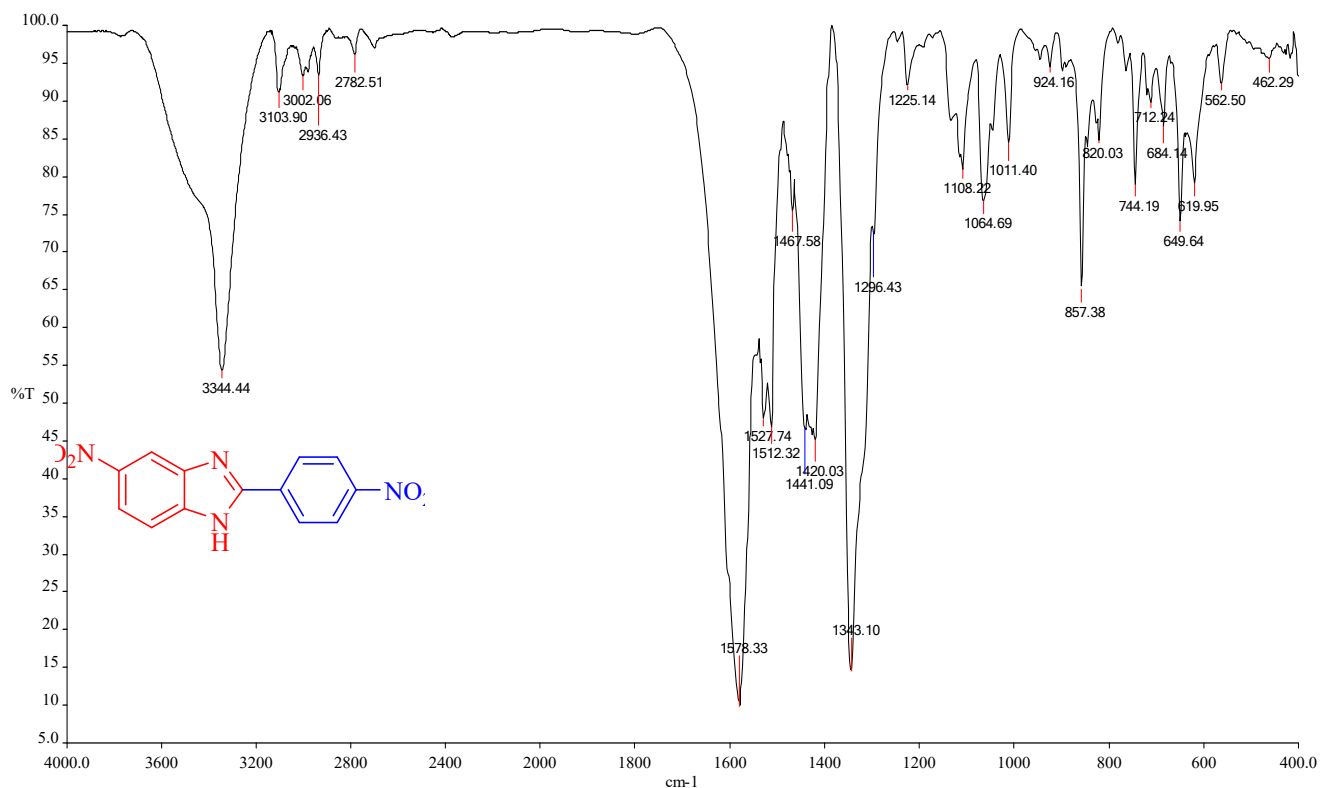


Figure S20. FT-IR spectrum of 5-nitro-2-(4-nitrophenyl)-1*H*-benzo[*d*]imidazole (**3d**) with KBr pellet

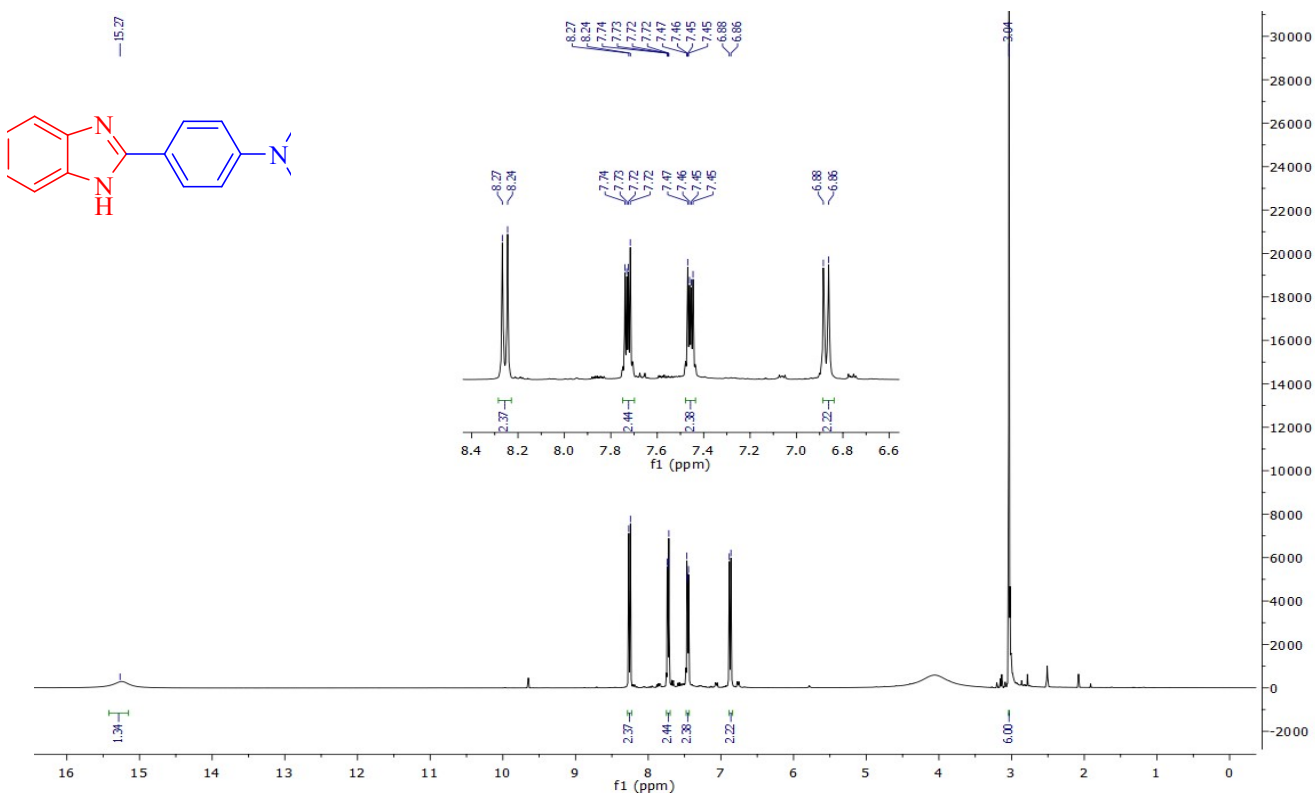


Figure S21. ¹H NMR of 4-(1*H*-benzo[*d*]imidazol-2-yl)-N, N-dimethylaniline (**3e**) in DMSO-*d*₆

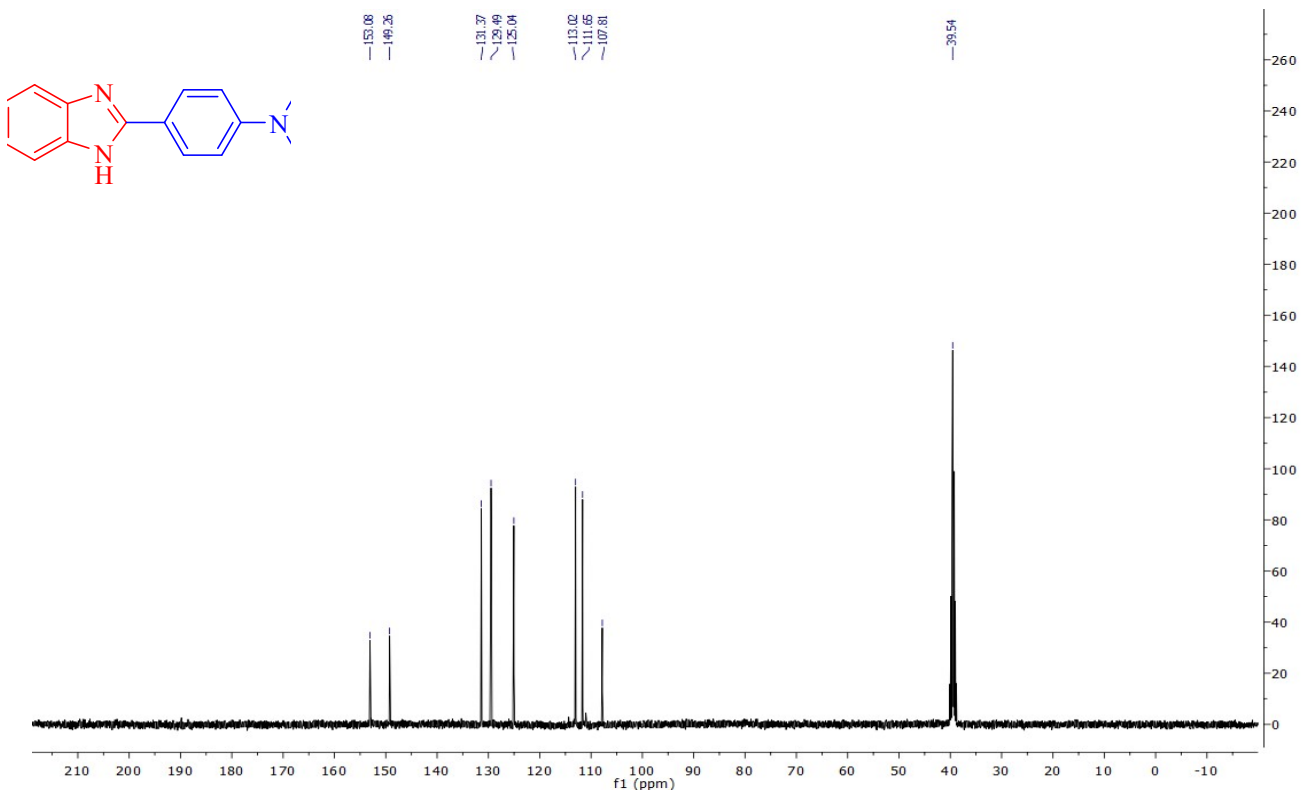


Figure S22. ¹³C NMR of 4-(1*H*-benzo[*d*]imidazol-2-yl)-N, N-dimethylaniline (**3e**) in DMSO-*d*₆

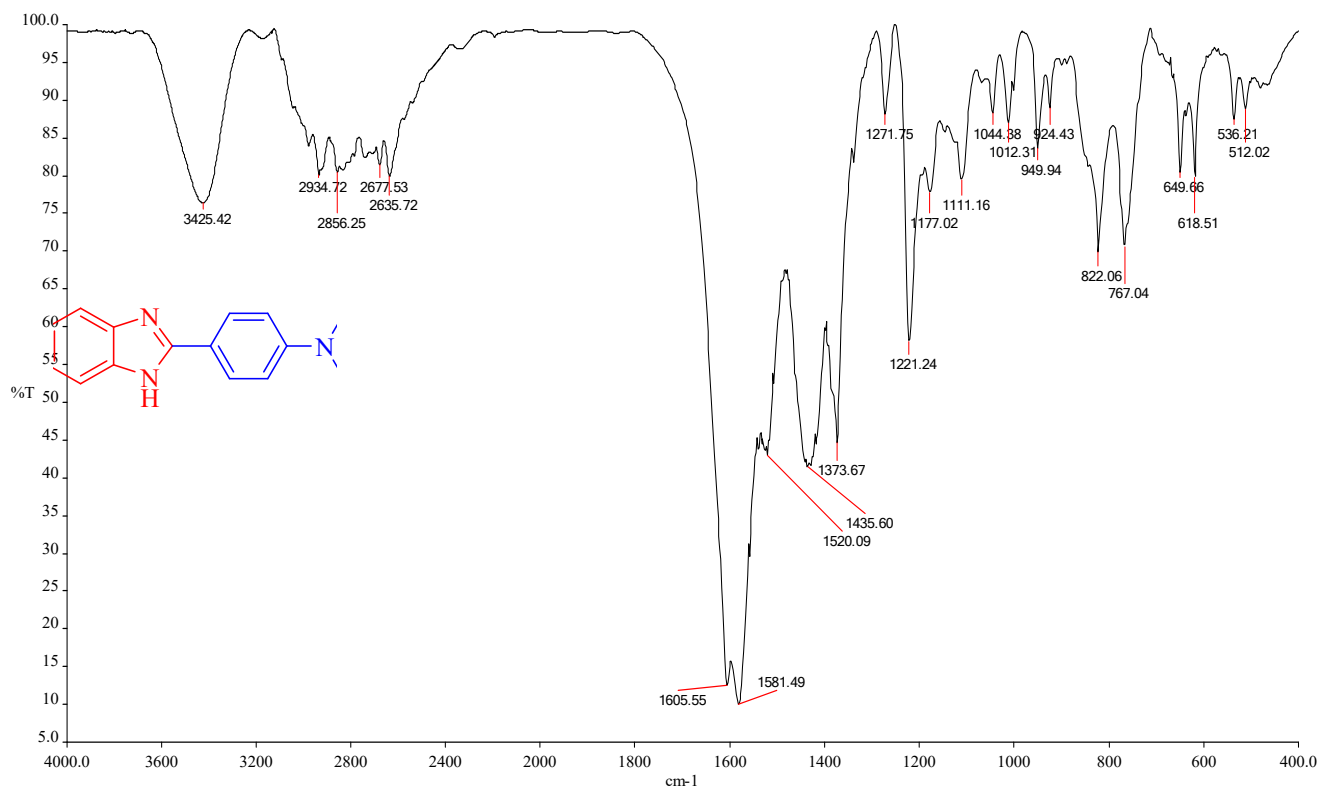


Figure S23. FT-IR spectrum of 4-(1*H*-benzo[*d*]imidazol-2-yl)-N, N-dimethylaniline (**3e**) with KBr pellet

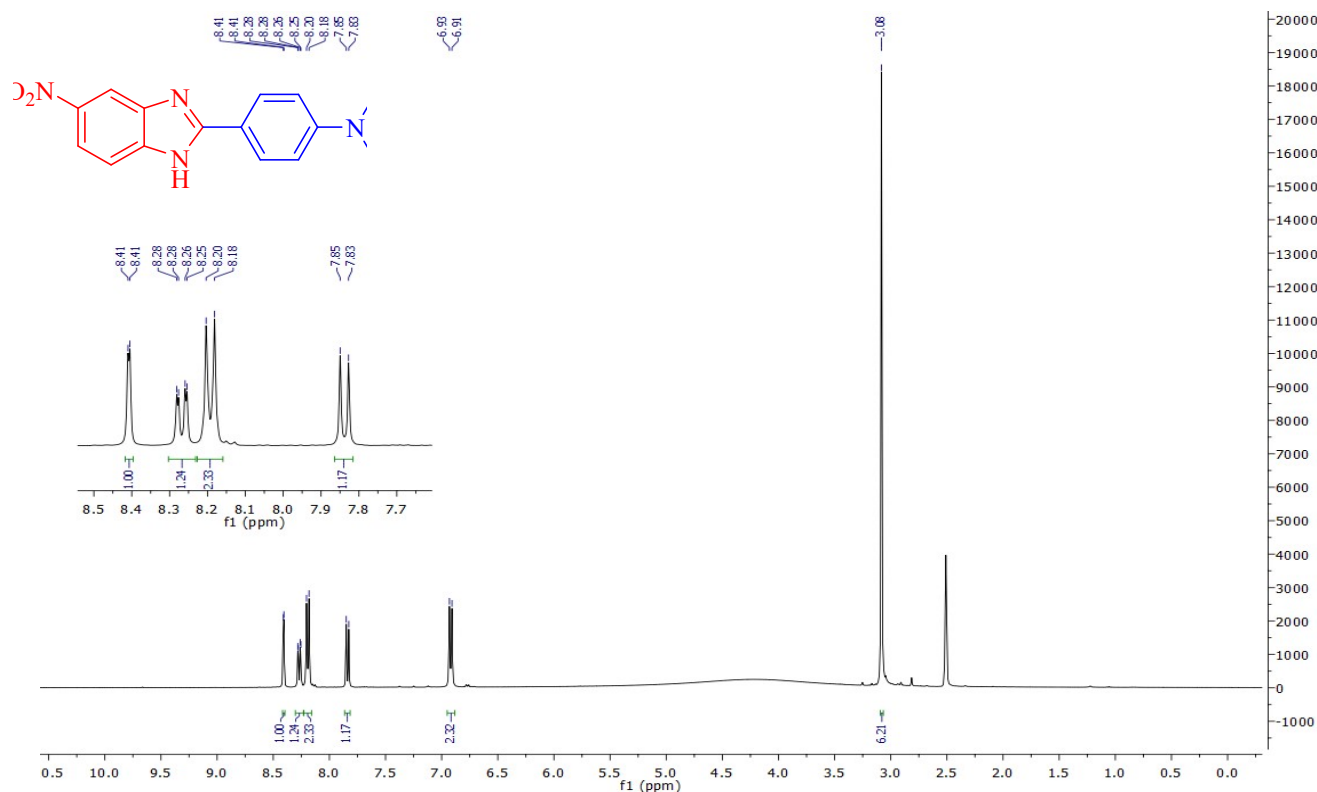


Figure S24. ¹H NMR of N, N-dimethyl-4-(5-nitro-1*H*-benzo[*d*]imidazol-2-yl) (**3f**) aniline in DMSO-*d*₆

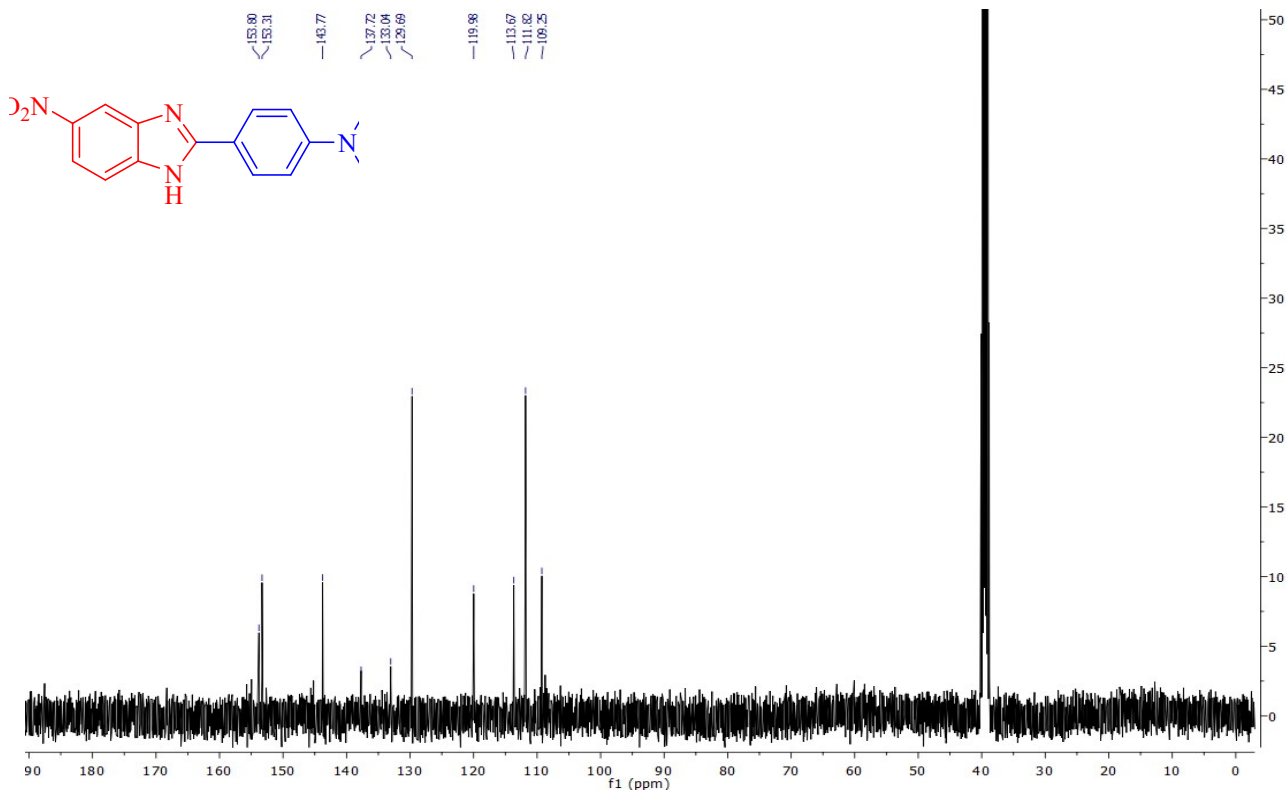


Figure S25. ^{13}C NMR of N, N-dimethyl-4-(5-nitro-1*H*-benzo[*d*]imidazol-2-yl) aniline (**3f**) in $\text{DMSO}-d_6$

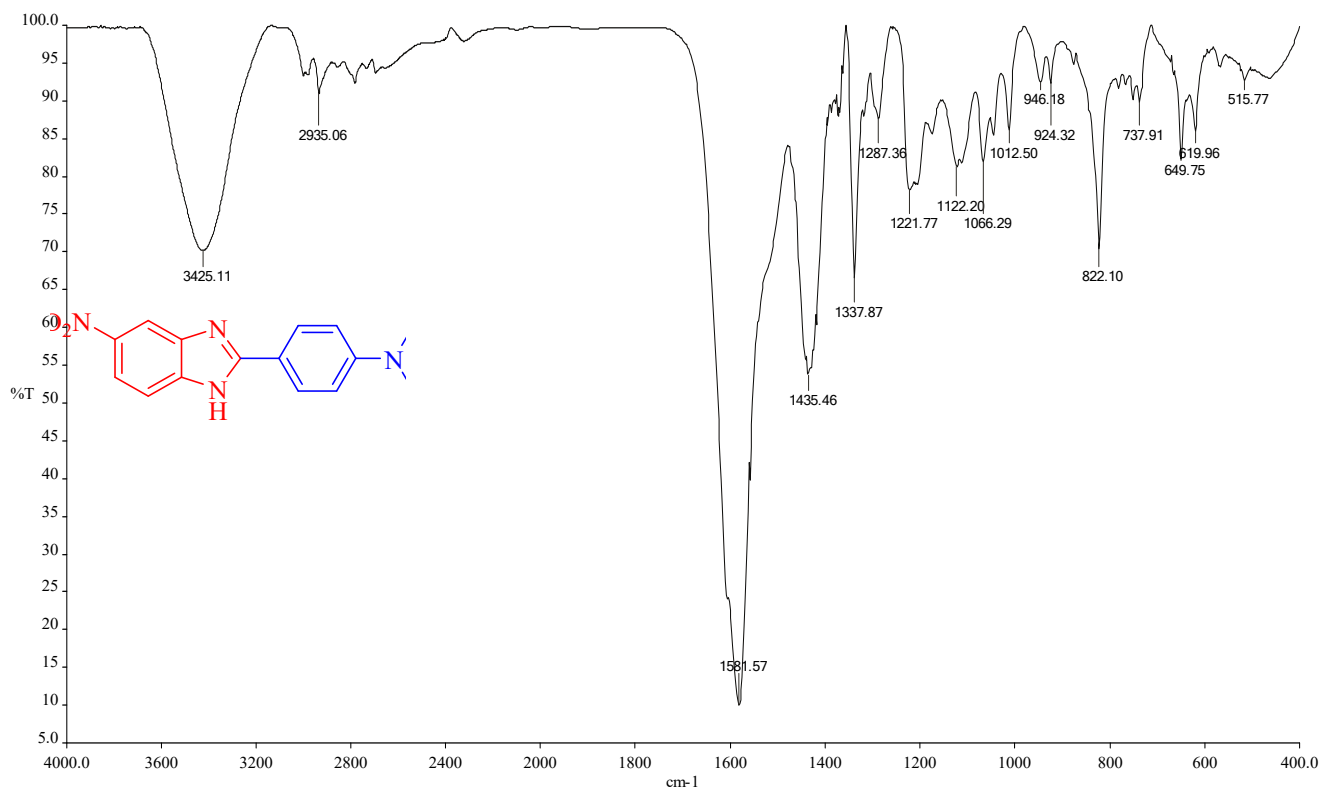


Figure S26. FT-IR spectrum of N, N-dimethyl-4-(5-nitro-1*H*-benzo[*d*]imidazol-2-yl) aniline (**3f**) with KBr pellet

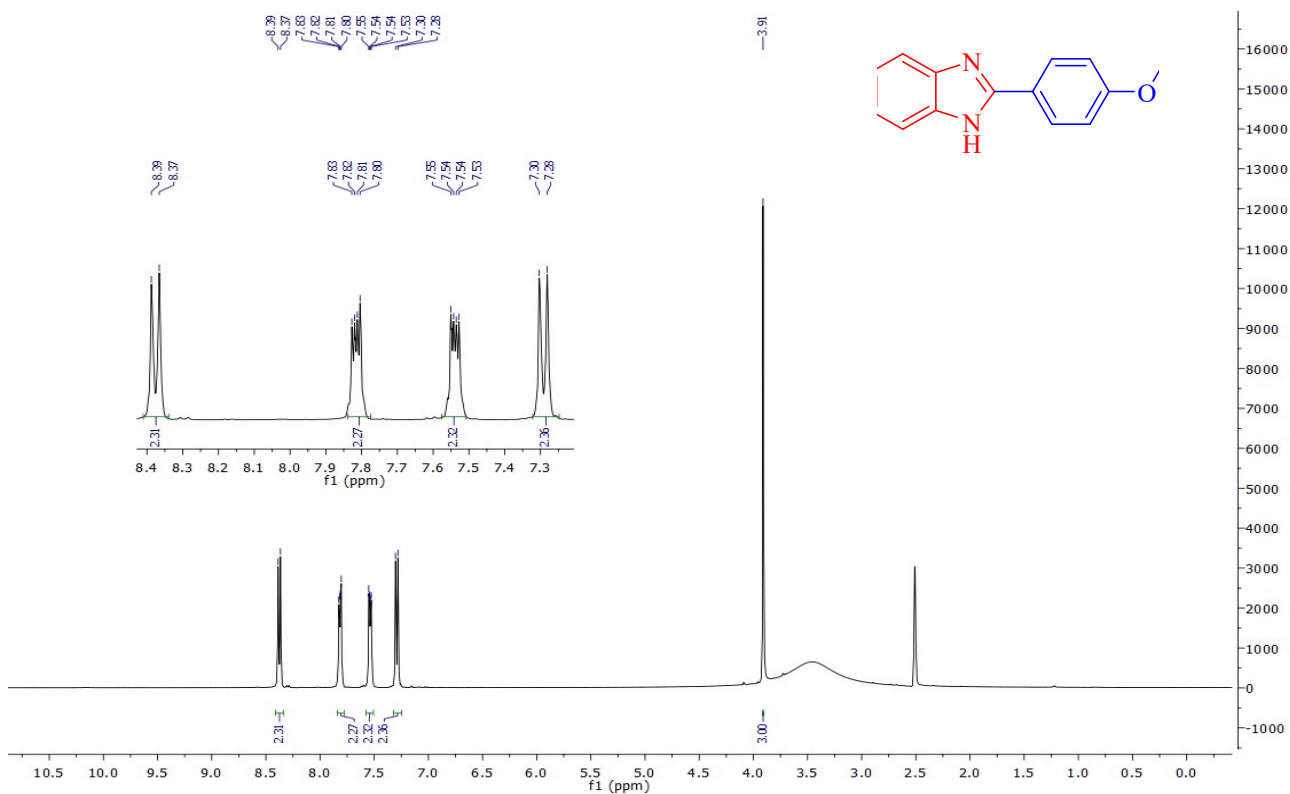


Figure S27. ^1H NMR of 2-(4-methoxyphenyl)-1*H*-benzo[*d*]imidazole (**3g**) in $\text{DMSO}-d_6$

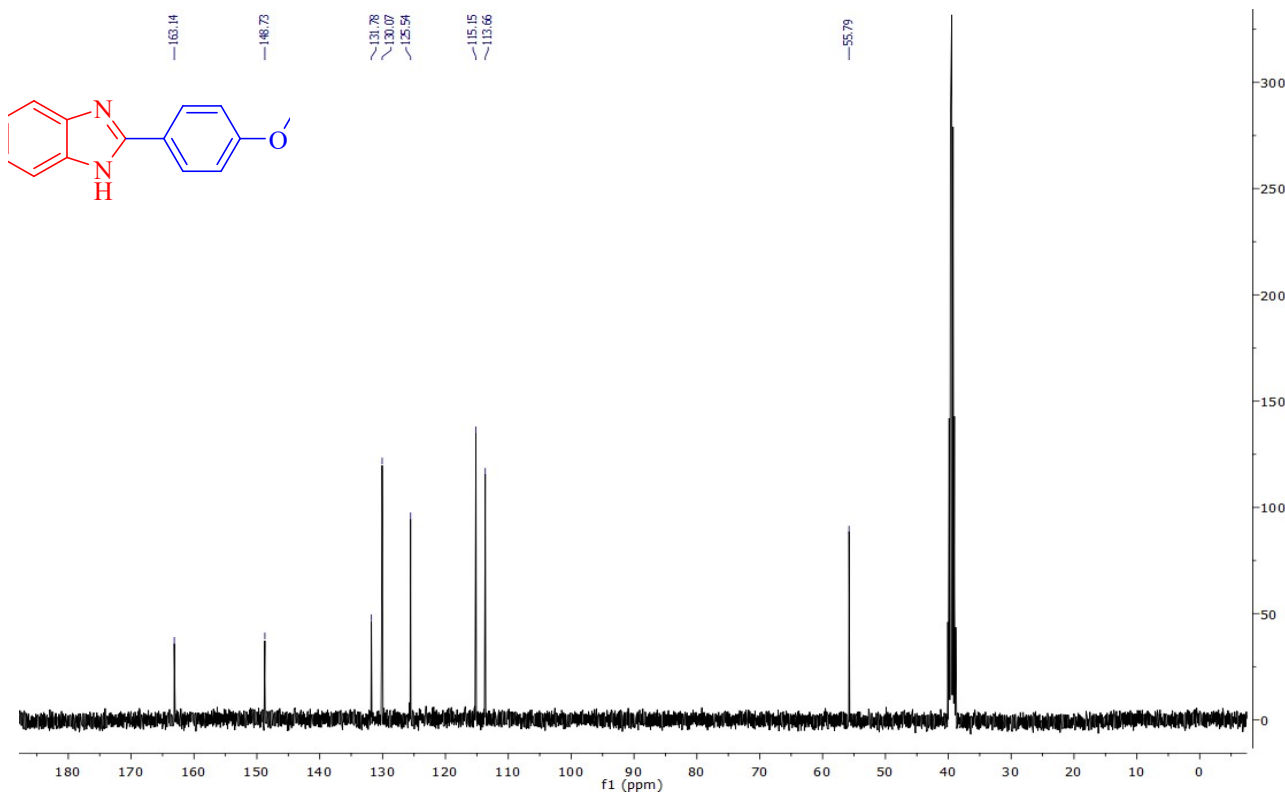


Figure S28. ^{13}C NMR of 2-(4-methoxyphenyl)-1*H*-benzo[*d*]imidazole (**3g**) in $\text{DMSO}-d_6$

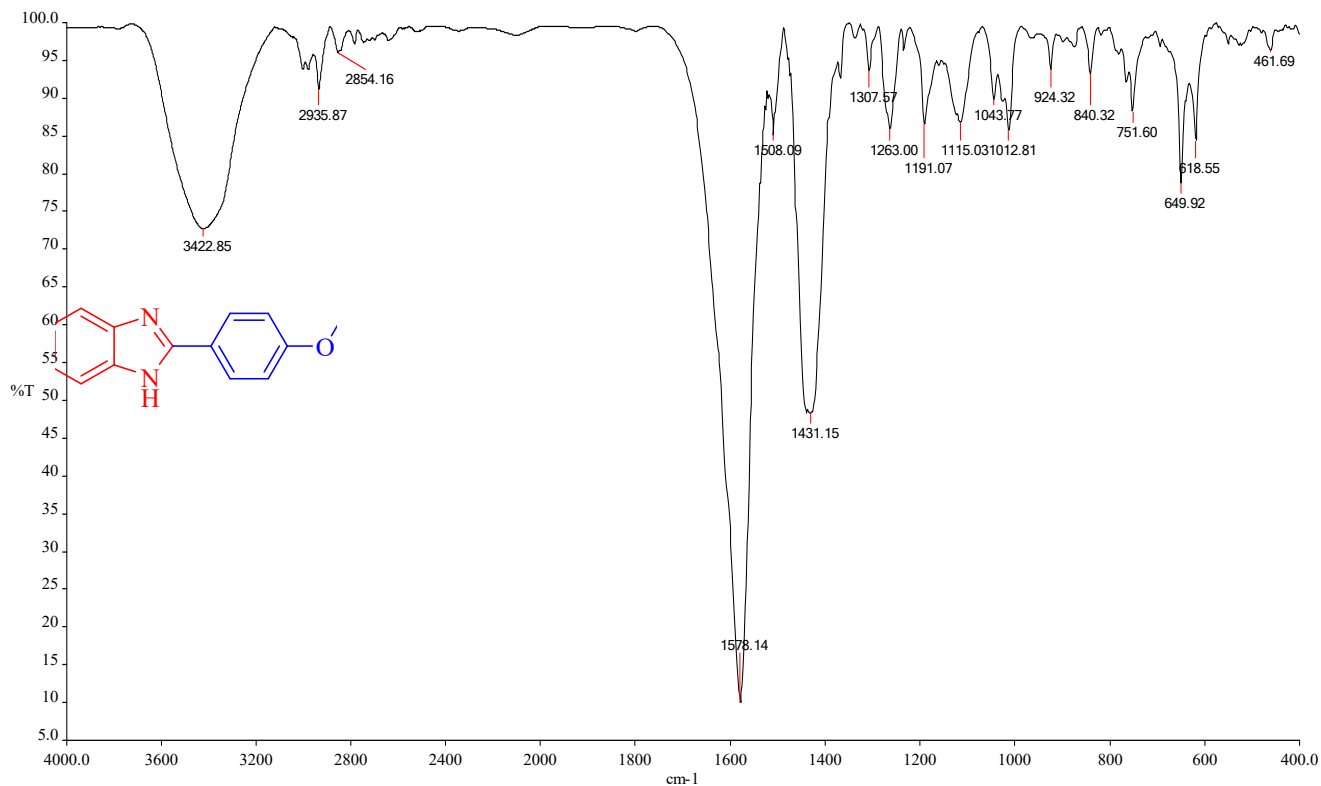


Figure S29. FT-IR spectrum of 2-(4-methoxyphenyl)-1*H*-benzo[*d*]imidazole (**3g**) with KBr pellet

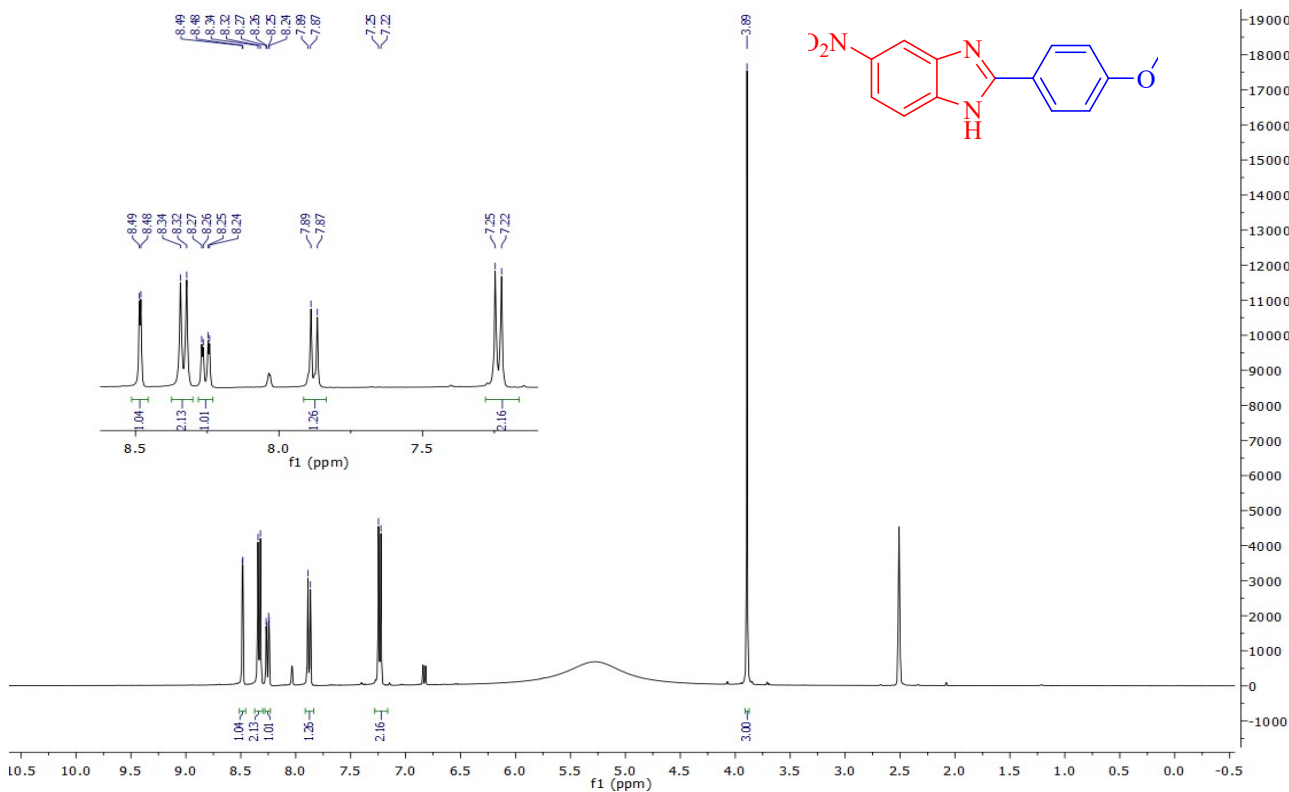


Figure S30. ^1H NMR of 2-(4-methoxyphenyl)-5-nitro-1*H*-benzo[*d*]imidazole (**3h**) in $\text{DMSO}-d_6$

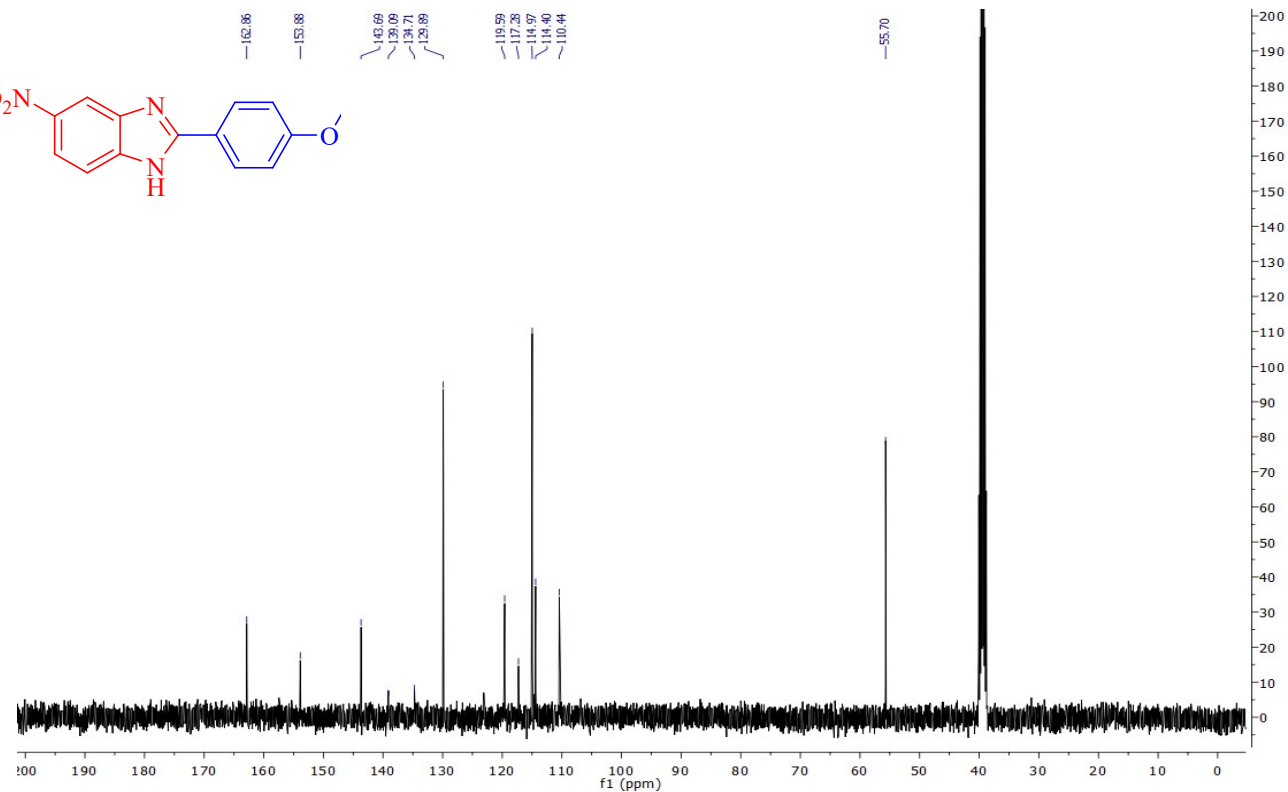


Figure S31. ^{13}C NMR of 2-(4-methoxyphenyl)-5-nitro-1*H*-benzo[*d*]imidazole (**3h**) in $\text{DMSO}-d_6$

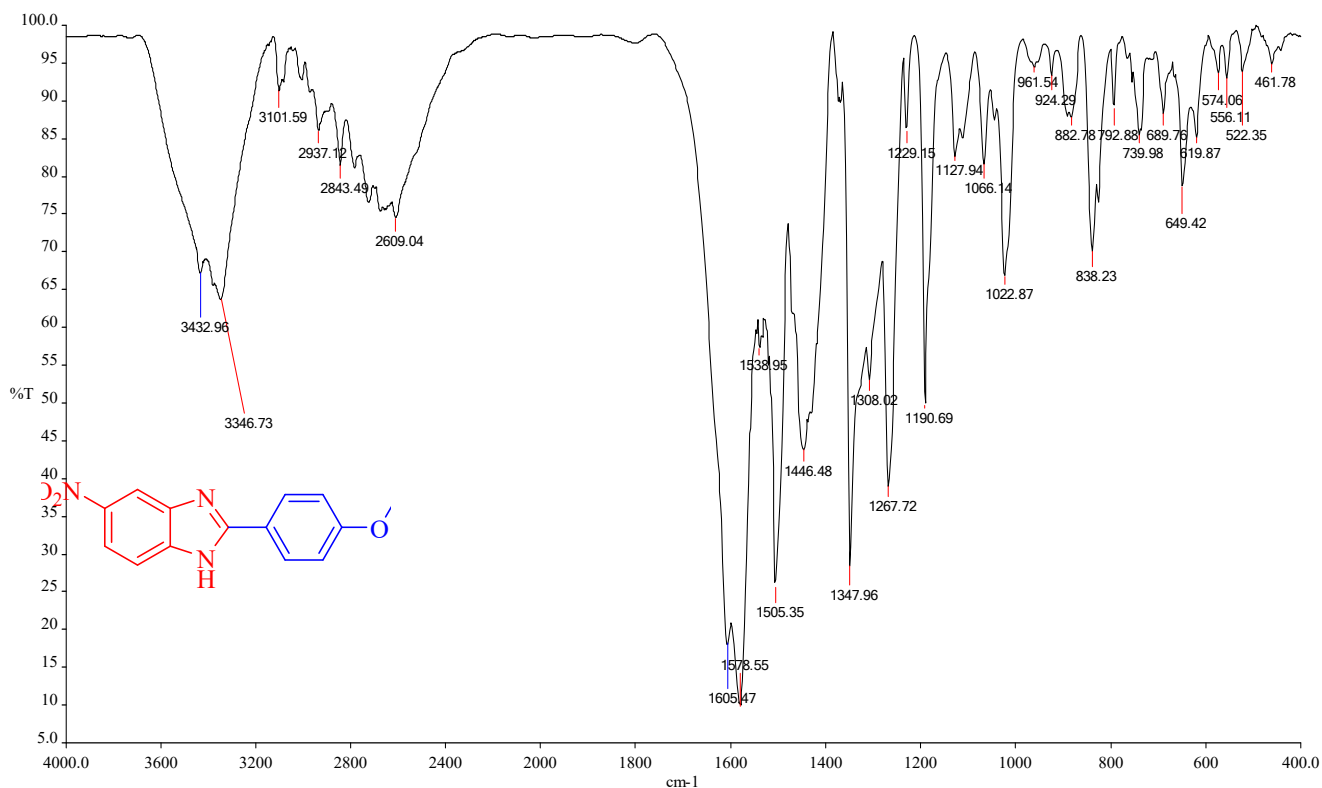


Figure S32. FT-IR spectrum of 2-(4-methoxyphenyl)-5-nitro-1*H*-benzo[*d*]imidazole (**3h**) with KBr pellet

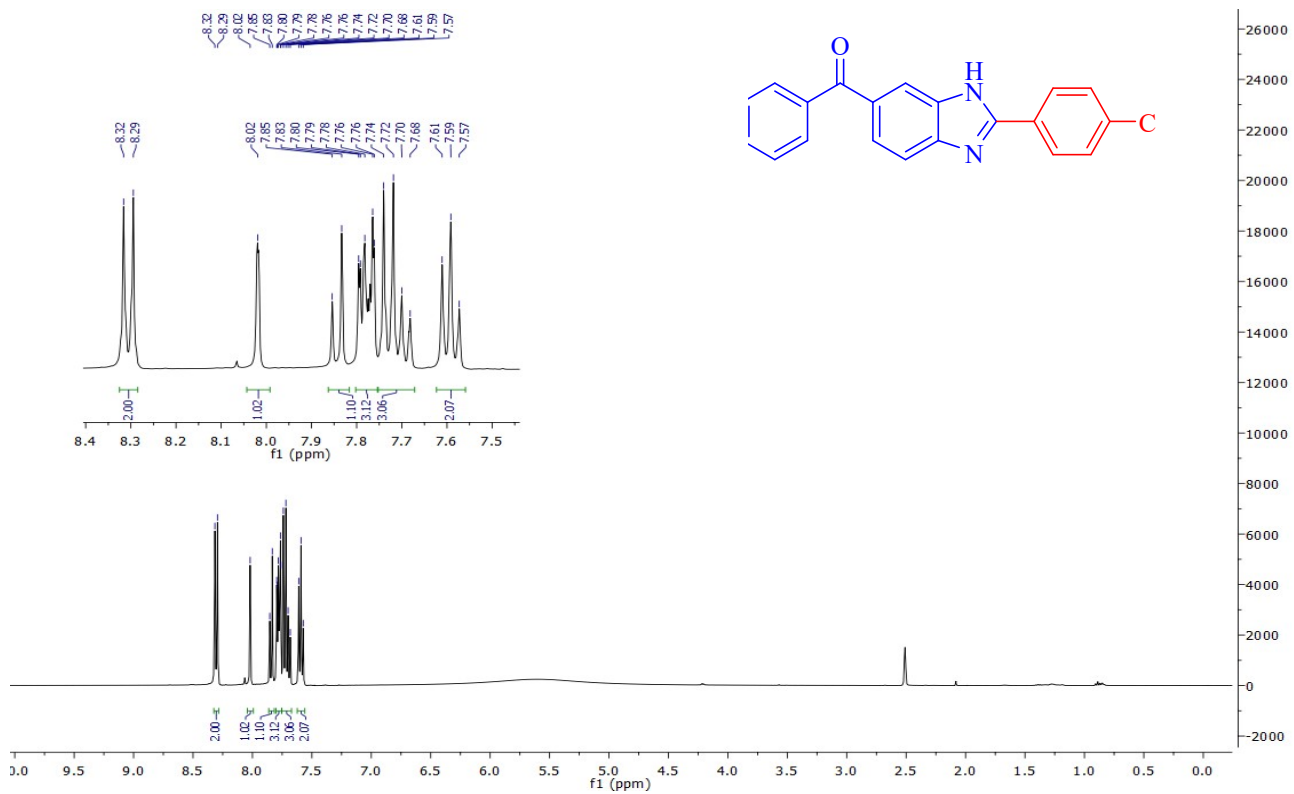


Figure S33. ^1H NMR of (2-(4-chlorophenyl)-1*H*-benzo[*d*]imidazol-6-yl) (phenyl)methanone (**3i**) in $\text{DMSO}-d_6$

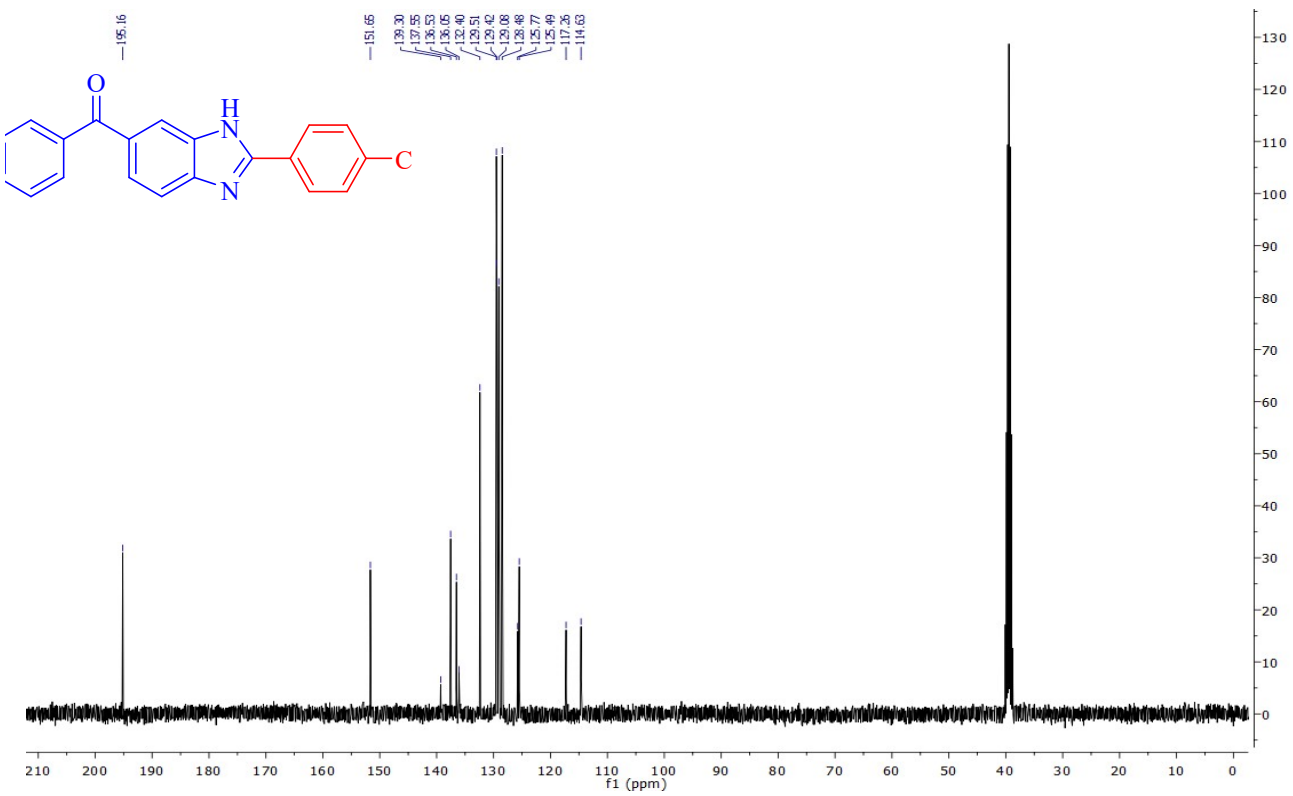


Figure S34. ^{13}C NMR of (2-(4-chlorophenyl)-1*H*-benzo[*d*]imidazol-6-yl) (phenyl)methanone (**3i**) in $\text{DMSO}-d_6$

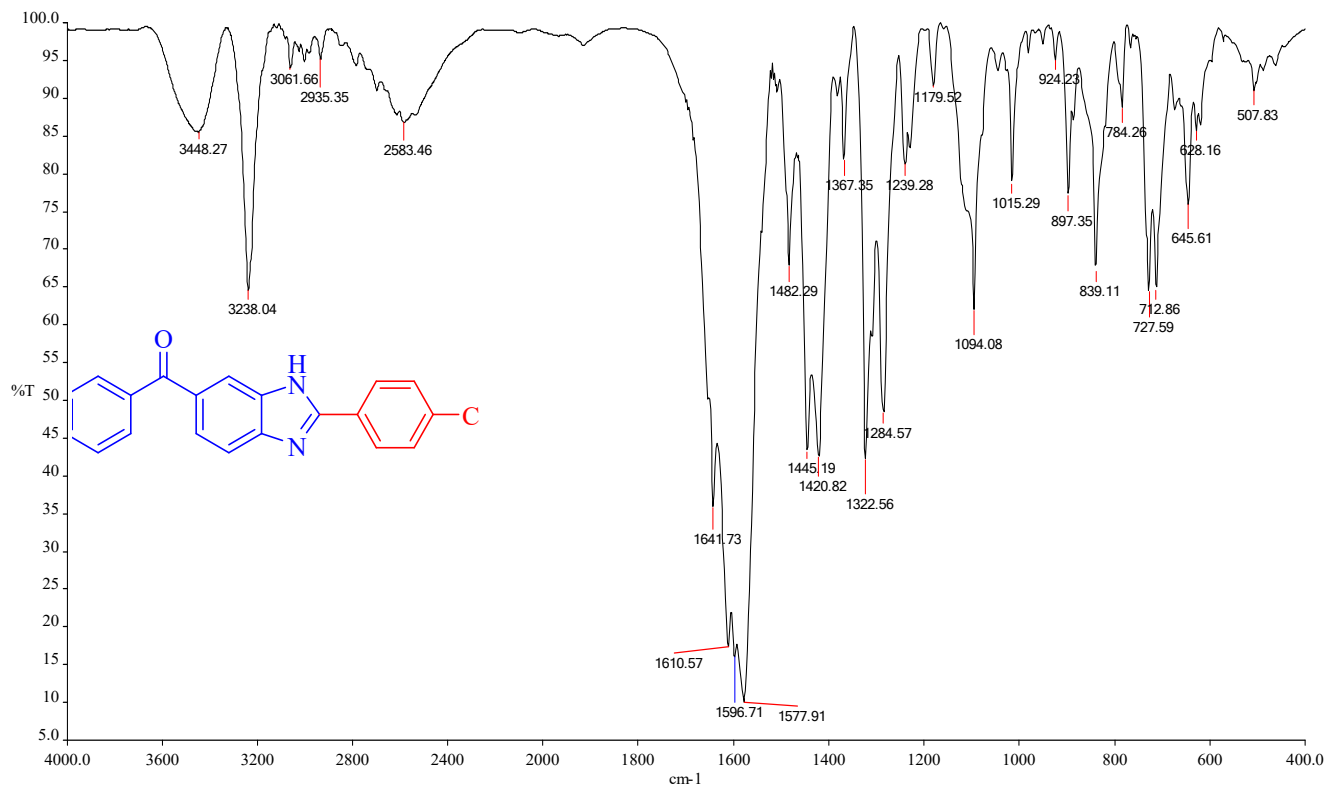


Figure S35. FT-IR spectrum of (2-(4-chlorophenyl)-1*H*-benzo[*d*]imidazol-6-yl) (phenyl)methanone (**3i**) with KBr pellet

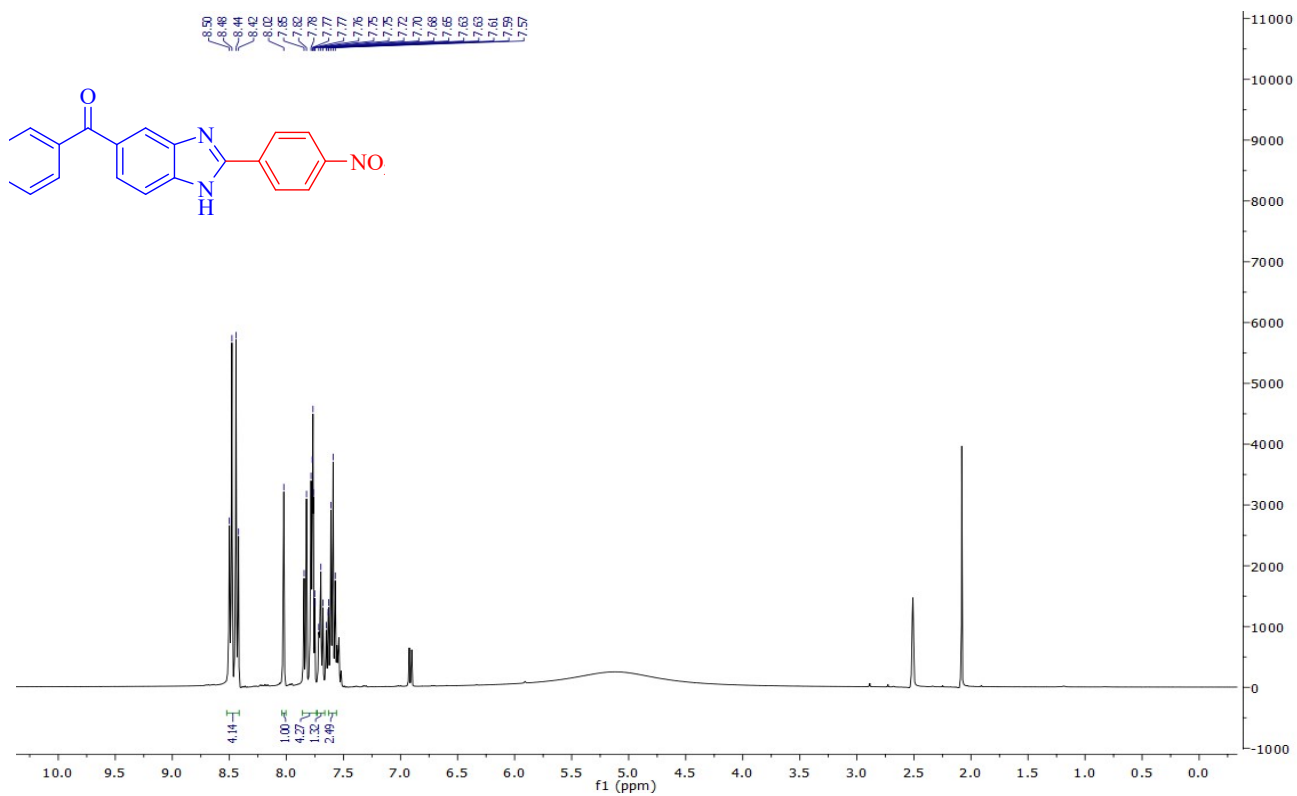


Figure S36. ^1H NMR of (2-(4-nitrophenyl)-1*H*-benzo[*d*]imidazol-5-yl) (phenyl)methanone (**3j**) in $\text{DMSO}-d_6$

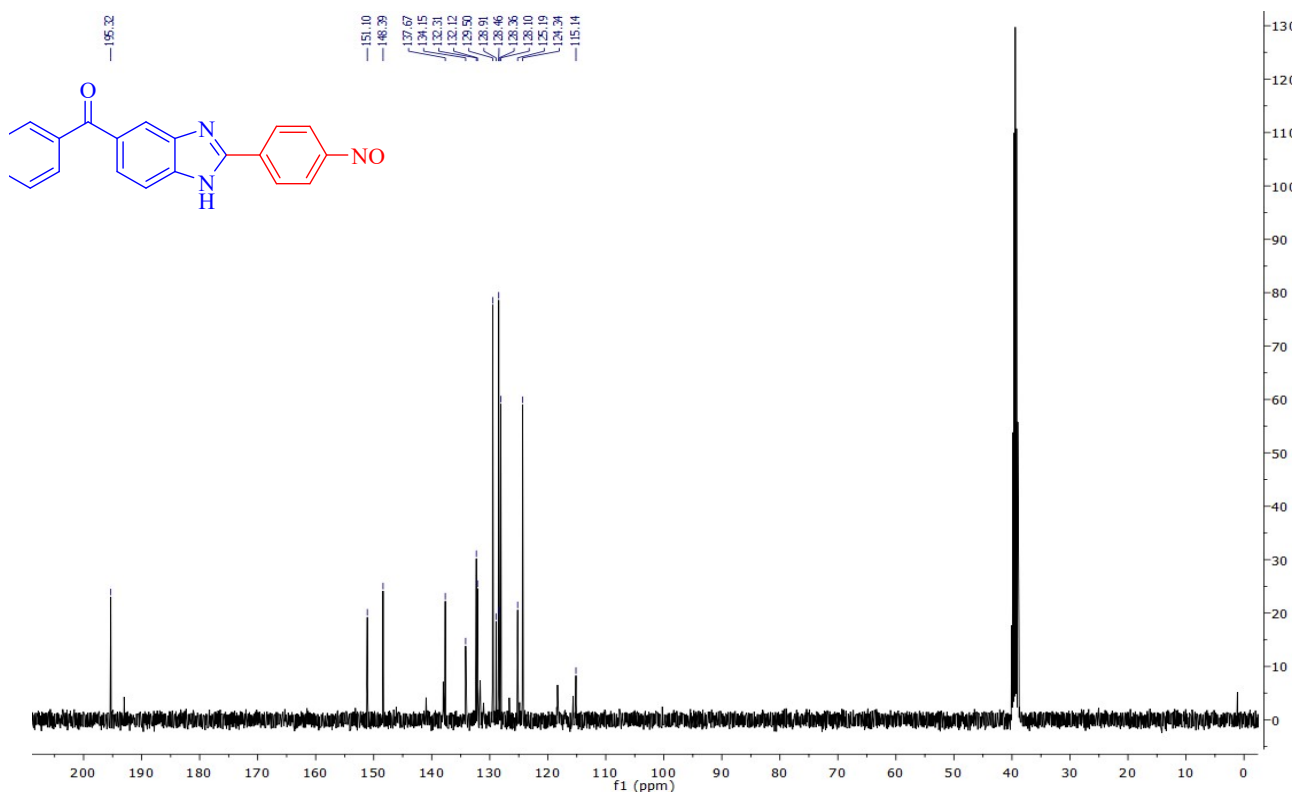


Figure S37. ^{13}C NMR of (2-(4-nitrophenyl)-1*H*-benzo[*d*]imidazol-5-yl) (phenyl)methanone (**3j**) in $\text{DMSO}-d_6$

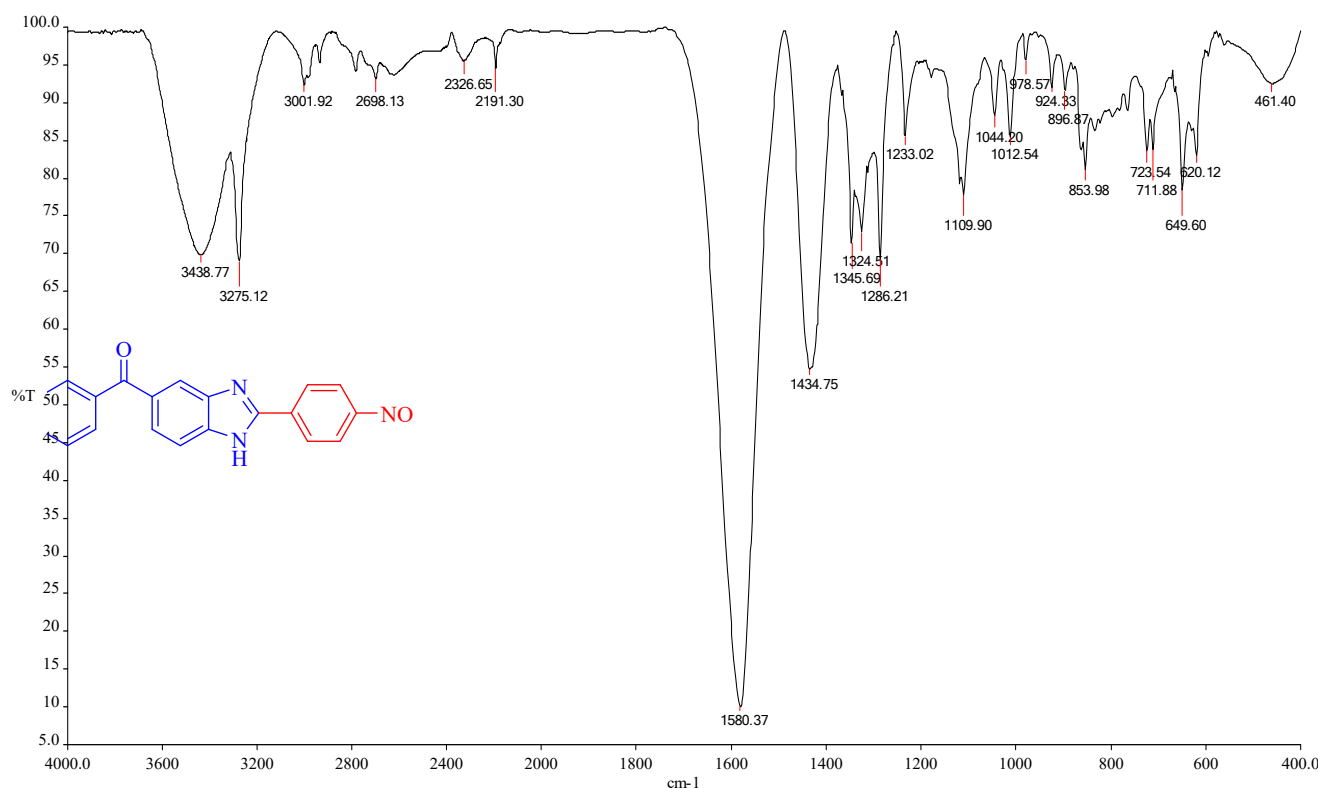


Figure S38. FT-IR spectrum of (2-(4-nitrophenyl)-1*H*-benzo[*d*]imidazol-5-yl) (phenyl)methanone (**3j**) with KBr pellet

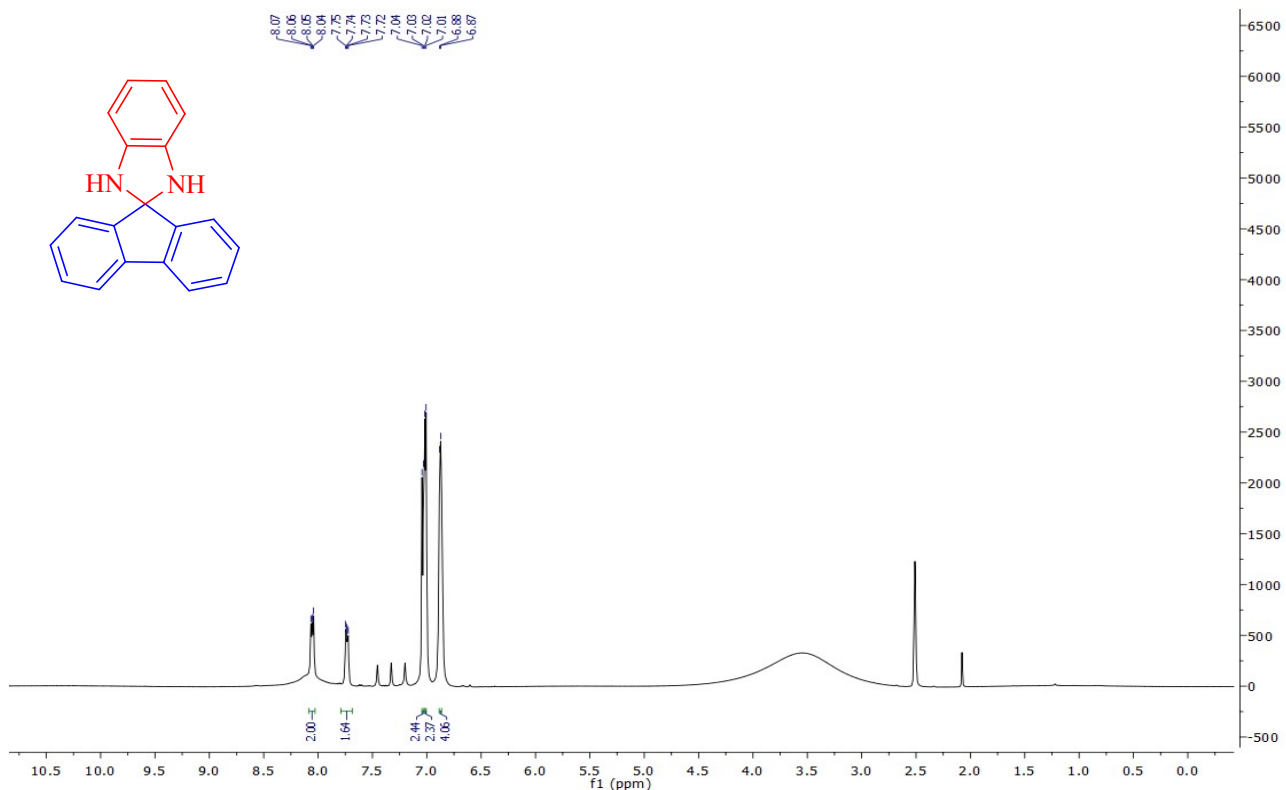


Figure S39. ¹H NMR of 1,3-dihydrospiro[benzo[*d*]imidazole-2,9'-fluorene] (**3k**) in DMSO-*d*₆

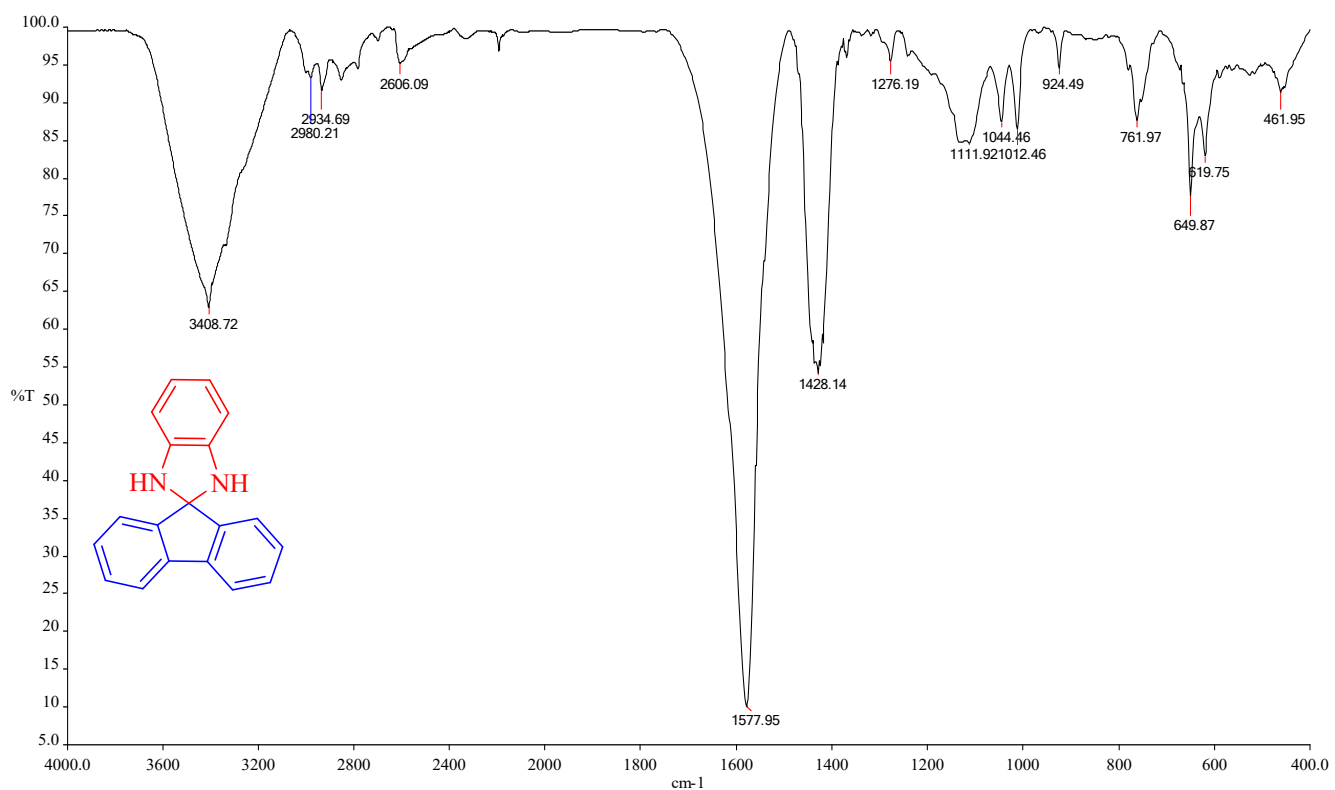


Figure S40. FT-IR spectrum of 1,3-dihydrospiro[benzo[*d*]imidazole-2,9'-fluorene] (**3k**) with KBr pellet

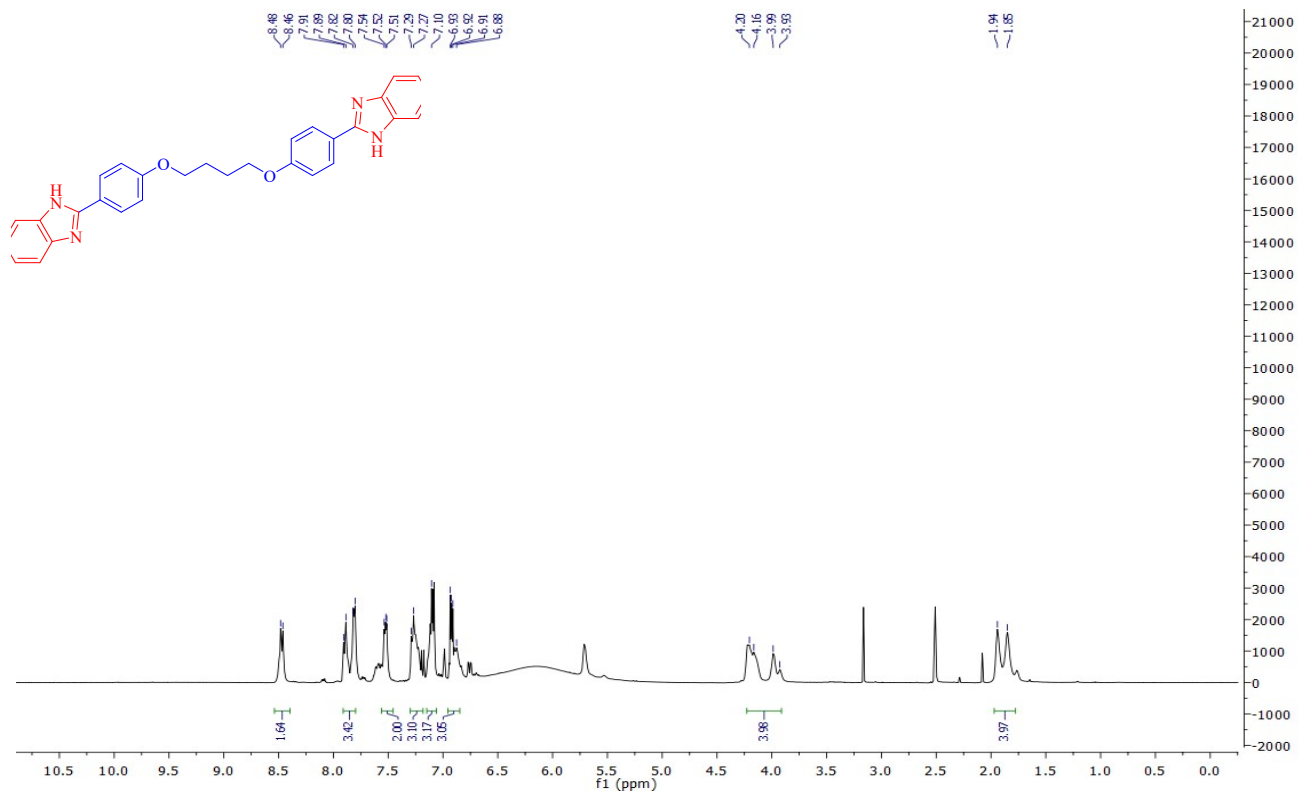


Figure S41. ^1H NMR of 1,4-bis(4-(1*H*-benzo[*d*]imidazol-2-yl) phenoxy) butane (**3l**) in $\text{DMSO}-d_6$

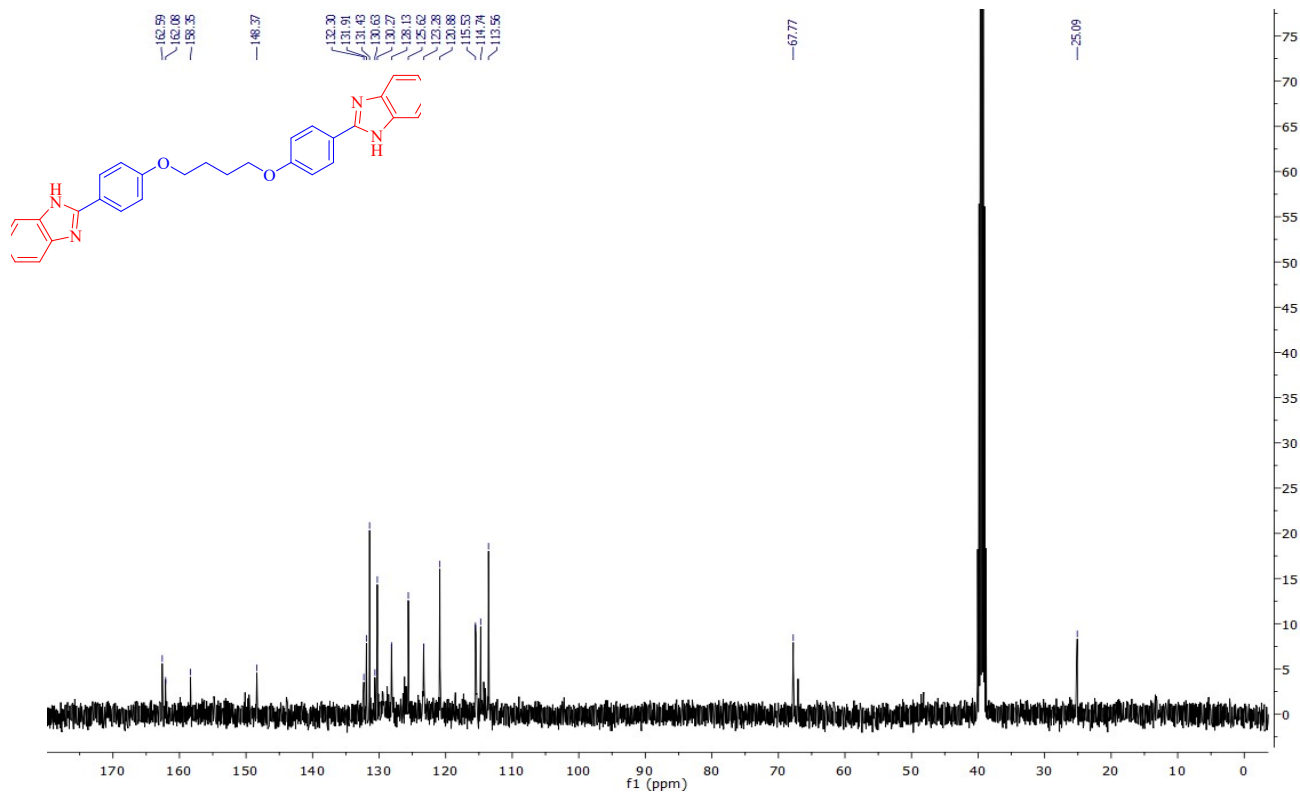


Figure S42. ^{13}C NMR of 1,4-bis(4-(1*H*-benzo[*d*]imidazol-2-yl) phenoxy) butane (**3l**) in $\text{DMSO}-d_6$

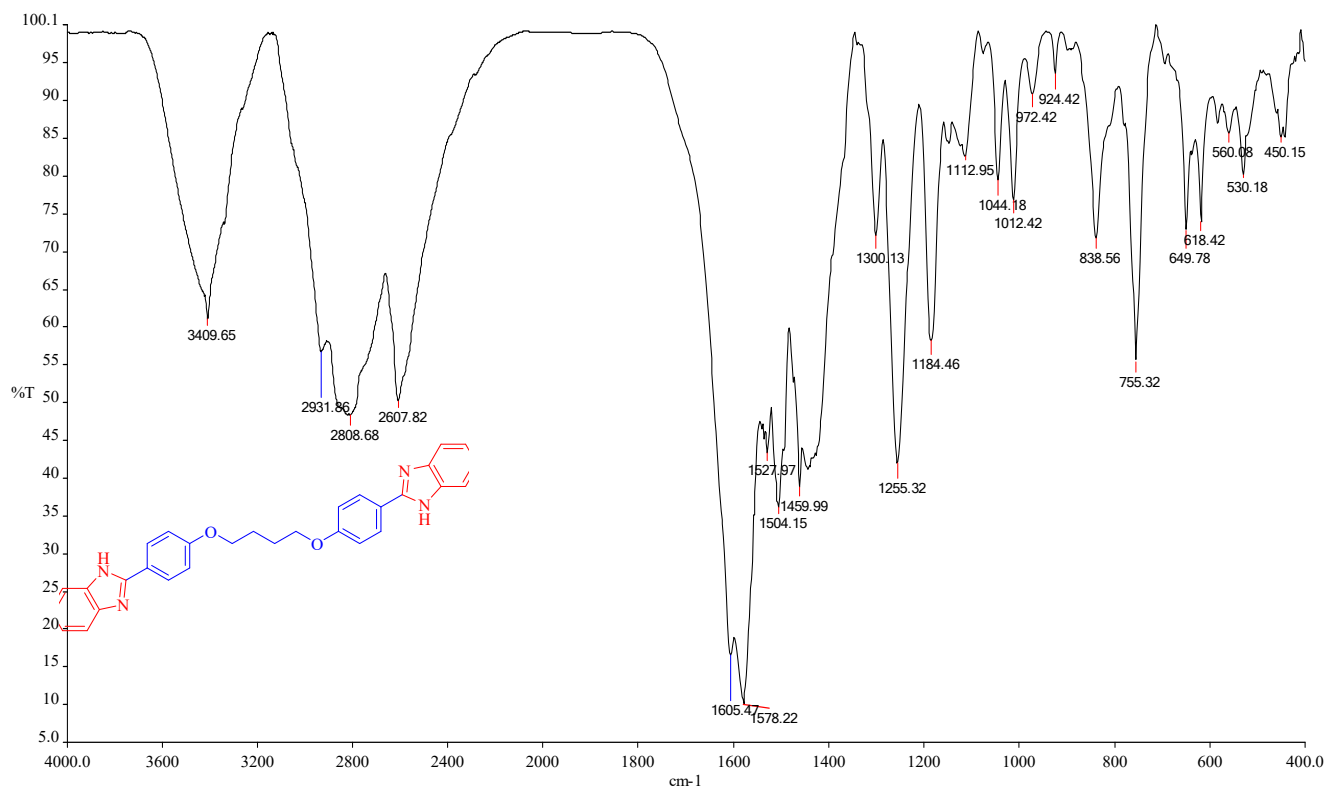


Figure S43. FT-IR spectrum of 1,4-bis(4-(1*H*-benzo[*d*]imidazol-2-yl) phenoxy) butane (**3l**) with KBr pellet

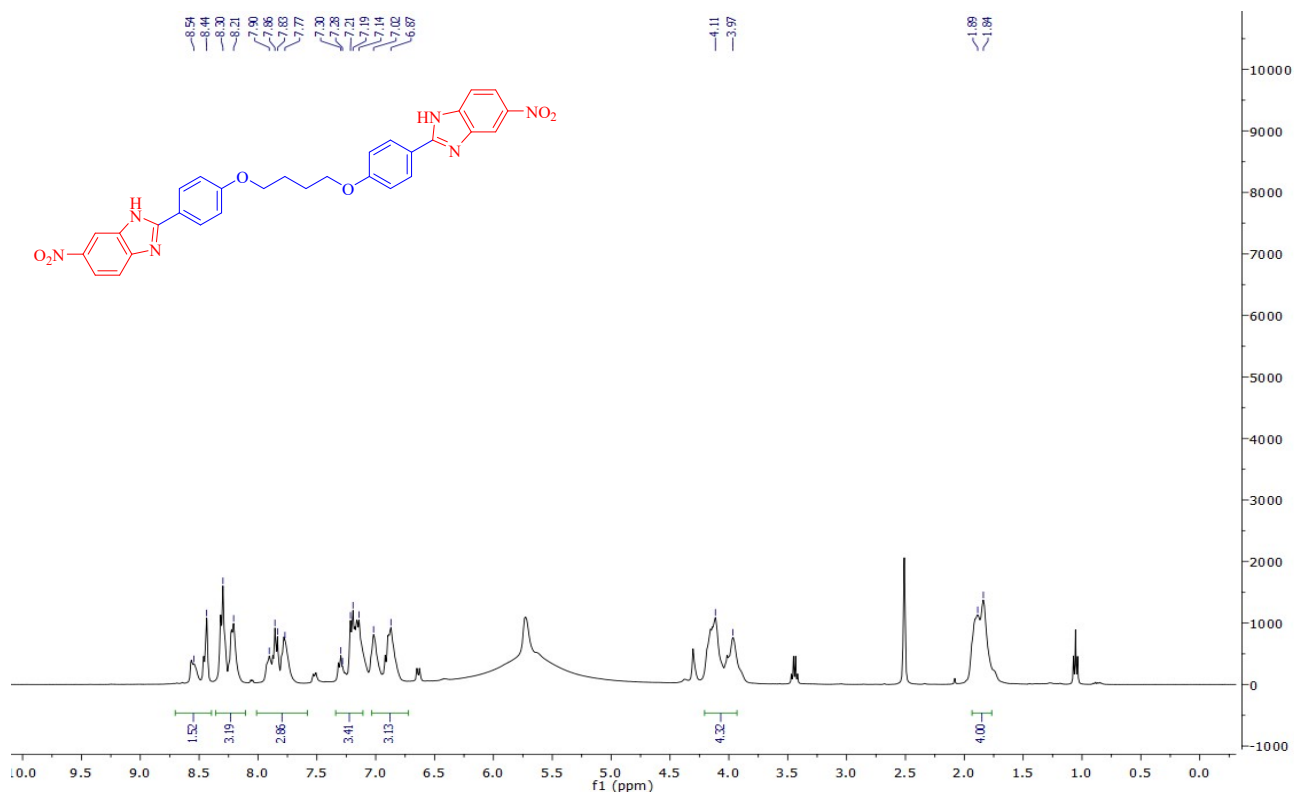


Figure S44. ¹H NMR of 6-nitro-2-(4-(4-(5-nitro-1*H*-benzo[*d*]imidazol-2-yl)phenoxy)butoxy)phenyl-1*H*-benzo[*d*] imidazole (**3m**) in DMSO-*d*₆

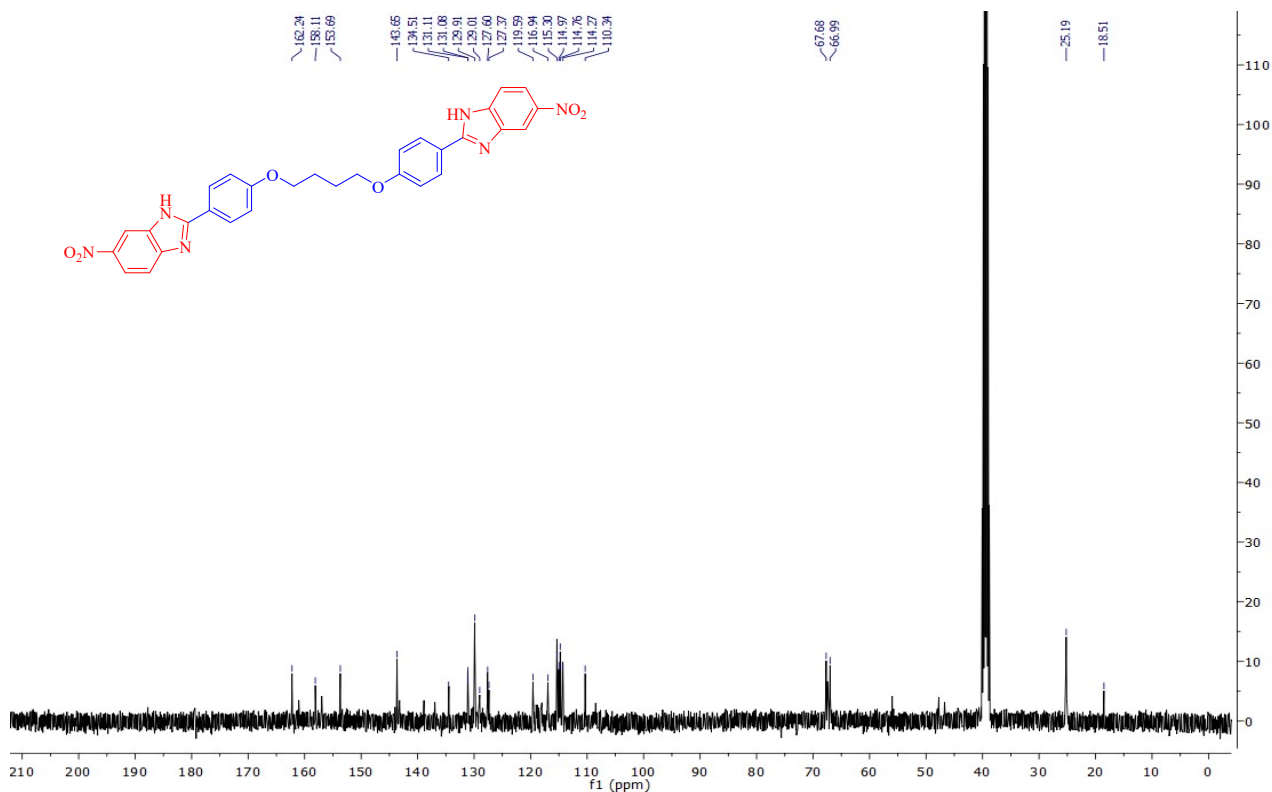


Figure S45. ^{13}C NMR of 6-nitro-2-(4-(4-(5-nitro-1*H*-benzo[*d*]imidazol-2-yl)phenoxy)butoxy)phenyl)-1*H*-benzo[*d*] imidazole (**3m**) in $\text{DMSO}-d_6$

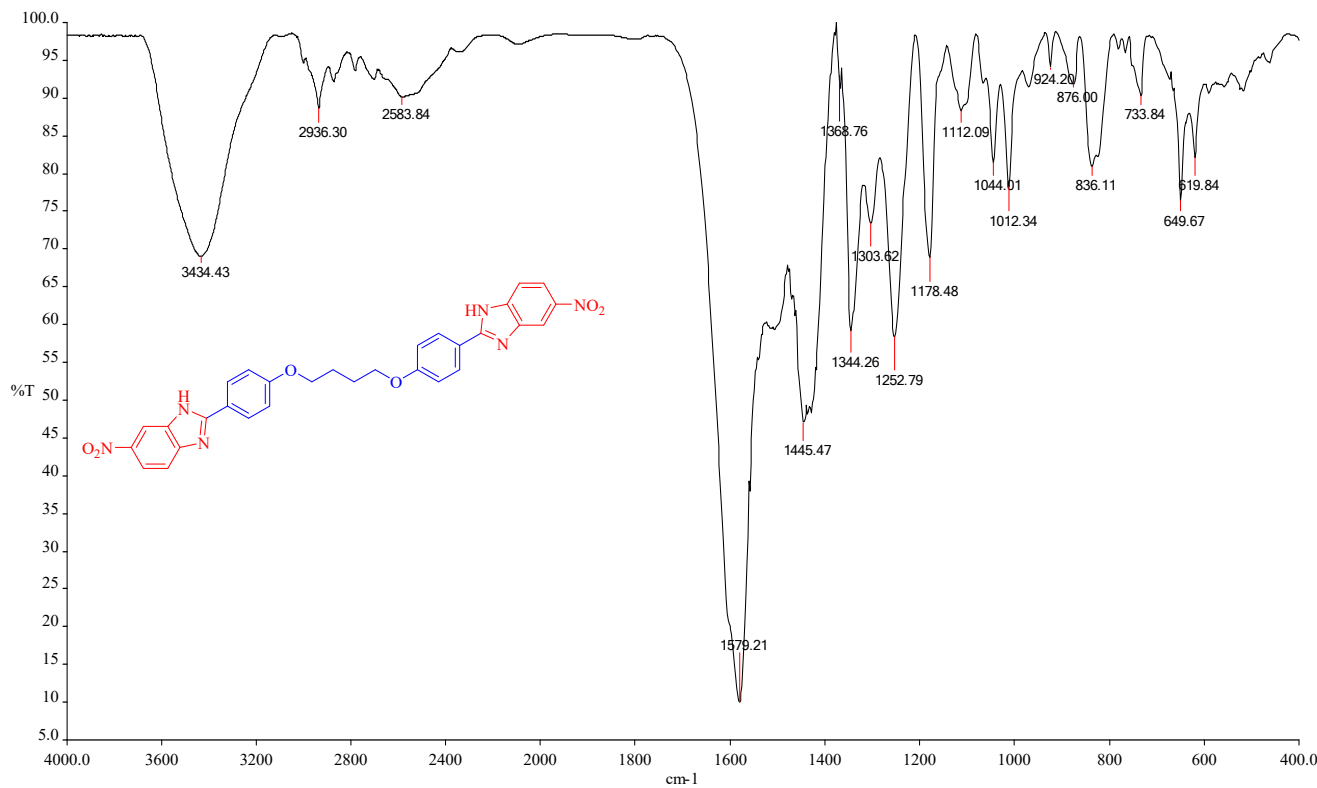


Figure S46. FT-IR spectrum of 6-nitro-2-(4-(4-(5-nitro-1*H*-benzo[*d*]imidazol-2-yl)phenoxy)butoxy)phenyl)-1*H*-benzo[*d*] imidazole (**3m**) with KBr pellet

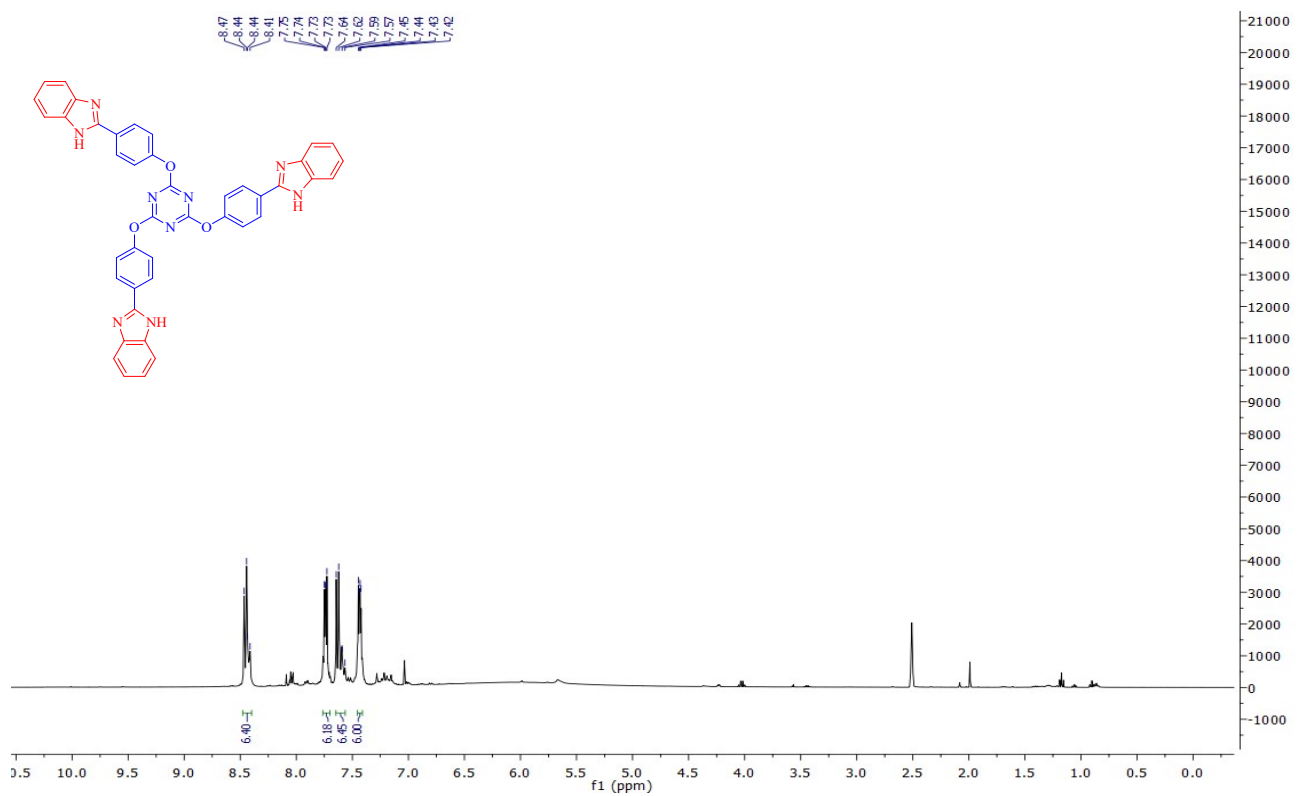


Figure S47. ^1H NMR of 2,4,6-tris(4-(1*H*-benzo[*d*]imidazol-2-yl) phenoxy)-1,3,5-triazine (**3n**) in $\text{DMSO}-d_6$

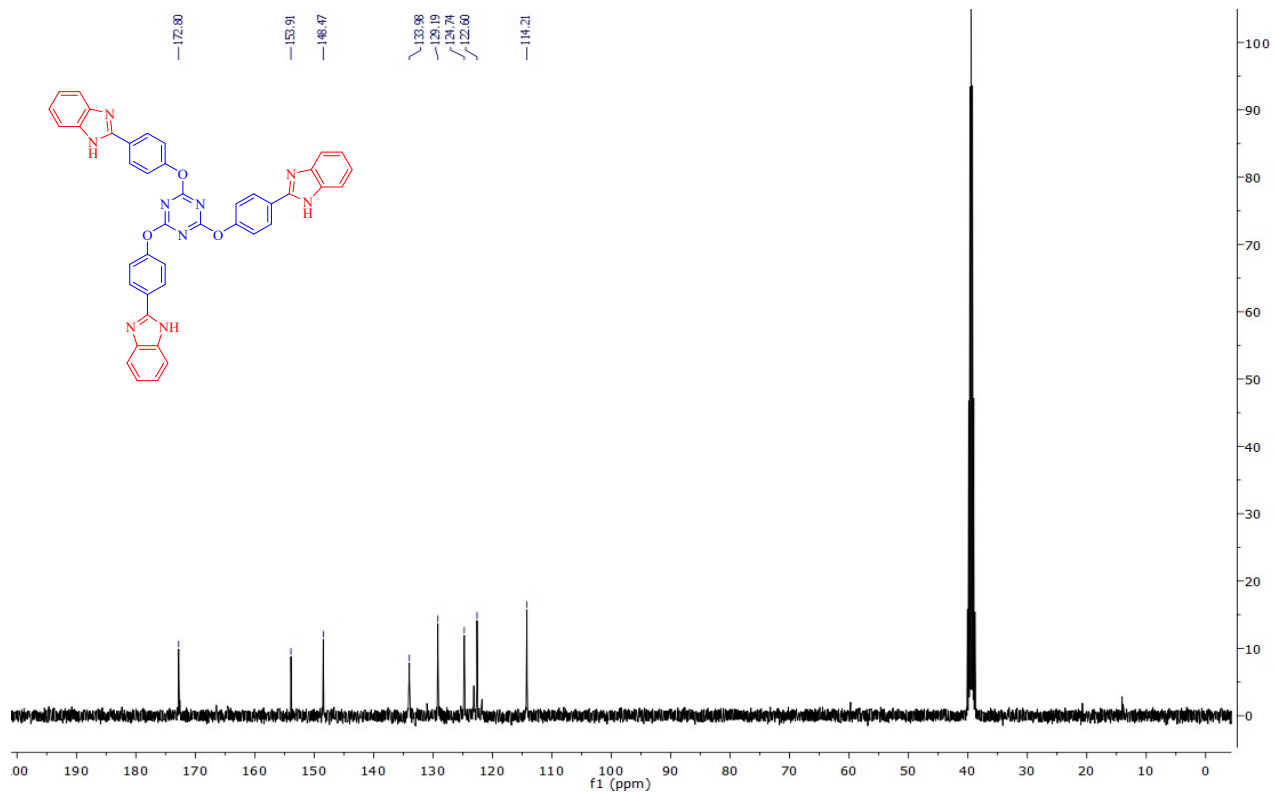


Figure S48. ^{13}C NMR of 2,4,6-tris(4-(1*H*-benzo[*d*]imidazol-2-yl) phenoxy)-1,3,5-triazine (**3n**) in $\text{DMSO}-d_6$

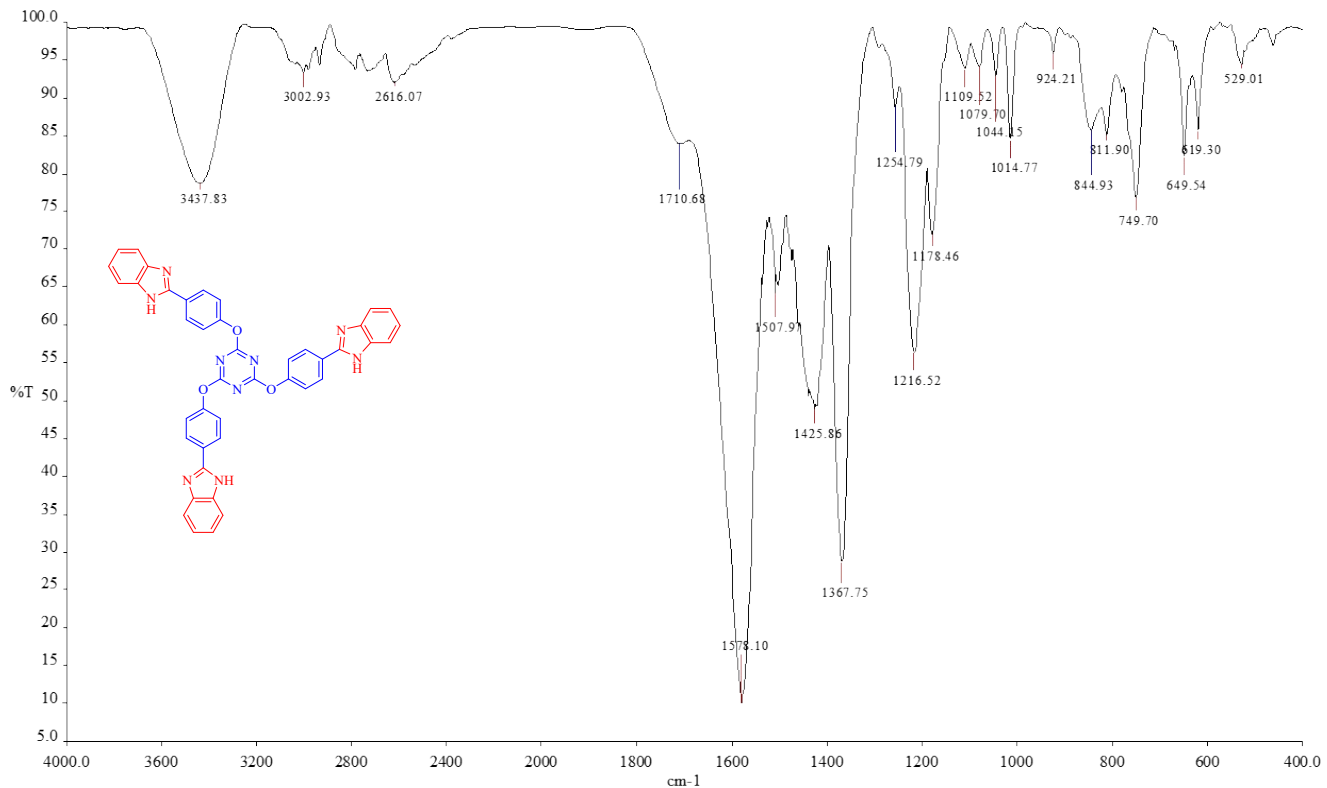


Figure S49. FT-IR spectrum of 2,4,6-tris(4-(1*H*-benzo[*d*]imidazol-2-yl) phenoxy)-1,3,5-triazine (**3n**) with KBr pellet

Refrencess:

1. C. C. Le, M. K. Wismer, Z.-C. Shi, R. Zhang, D. V. Conway, G. Li, P. Vachal, I. W. Davies and D. W. MacMillan, *ACS central science*, 2017, **3**, 647-653.
2. M. Bashiri, A. Jarrahpour, S. M. Nabavizadeh, S. Karimian, B. Rastegari, E. Haddadi and E. Turos, *Medicinal Chemistry Research*, 2021, **30**, 258-284.
3. M. Bashiri, A. Jarrahpour, B. Rastegari, A. Iraji, C. Irajie, Z. Amirghofran, S. Malek-Hosseini, M. Motamedifar, M. Haddadi and K. Zomorodian, *Monatshefte für Chemie-Chemical Monthly*, 2020, **151**, 821-835.